University of Cincinnati

Date: 7/16/2018

I, Purva Bhatnagar, hereby submit this original work as part of the requirements for the degree of Doctor of Philosophy in Electrical Engineering.

It is entitled:

Multi-Frequency and Multi-Sensor Impedance Sensing Platform for Biosensing Applications

Student's name: **Purva Bhatnagar**

This work and its defense approved by:

Committee chair: Fred Beyette, Ph.D.

Committee member: Jason Heikenfeld, Ph.D.

Committee member: Carla Purdy, Ph.D.

Committee member: Ryan White, Ph.D.

Committee member: Philip Wilsey, Ph.D.

30610

Multi-Frequency and Multi-Sensor Impedance Sensing Platform for Biosensing Applications

A thesis submitted to the Division of Research and Advanced Studies

of the University of Cincinnati

in partial fulfillment of the requirements for the degree of

DOCTOR OF PHILOSOPHY

in the school of Electrical Engineering and Computing Sciences

of the College of Engineering and Applied Sciences

July 2018

by

Purva Bhatnagar

MS Electrical Engineering

University of Cincinnati, Ohio, 2015

Thesis Advisor and Committee Chair: Dr. Fred R. Beyette Jr.

Abstract

The future of disease diagnostics and health care wearables lies in the development of low-cost sensors and devices that can detect minute traces of pathogens or antigens from body fluids. These devices will allow patients to run point of care diagnostics tests, thereby saving time and cost of running clinical tests and ultimately can provide early stage disease diagnosis and enable physicians to provide better-personalized treatment. There have been developments that focus on integrating multiple different tests into a single device that measures analytes from biofluids. Detection of glucose together with some single ions in a single device and test is the current attractive research advancement.

Electrochemistry Impedance Spectroscopy (EIS) is widely popular in the medical field where it is used to analyze biological materials as well as characterization of body fluids. It is a complex technique requiring expensive equipment that is also bulky making it difficult to integrate into small form-factor systems that are handheld, wearable and intended for use in point of care testing. This research work focused on developing a proof of concept prototype system with a flexible architecture that can be used for testing multiple sensors using EIS electroanalytical technique. The system is based on an embedded system design to be factored to achieve small valuation time for results along with being compact and portable enough to be used outside laboratory bench setting. The prototype successfully calculates the magnitude and phase of the impedance responses multiple electrochemical cells. The device transmits test data wirelessly to a personal computer or tablet which works together with an analysis and control display.

Acknowledgements

This thesis is dedicated to my loving parents, Aruna and Rakesh.

Staying in graduate school to complete a Doctoral thesis right after master's has been the best decision I have ever made. This journey has been long and sometimes demanding but has taught me so much while also giving me insight and appreciation towards life. This would not have been possible without my mentors, family, friends and colleagues, who have helped me at every step of my career.

I would like to begin by expressing my sincere gratitude to my advisor Dr. Fred R. Beyette Jr. for leading me in this amazing journey of research, mentorship and collaboration. Dr. Beyette's commitment and support towards my research, his technical abilities and great empathy makes him the best mentor I could have ever asked for. I will always be indebted to him for granting me an independent research environment to learn via failures and will always appreciate all the time he provided for our one-on-one meetings throughout the duration of the program.

My sincere thanks to Dr. Jason Heikenfeld for his constant guidance and unfaltering support on the progress of research. I would like to thank him for his valuable insights in shaping the validation and applications of my research work. I am grateful to Dr. Carla Purdy for always being forthcoming and making herself available for advice and inspiration. I am obliged to Dr. Philip Wilsey for taking me under his tutelage and for helping in identifying appropriate methodologies for tackling problems at hand. I am highly indebted to Dr. Ryan White for his willingness to readily collaborate and serve as a committee member towards end of my research. My sincere thanks to

him for taking the time to help me with data analysis and additional experiments. I am also thankful to Late Dr. William Connick for his contribution as a member of the dissertation committee and help in understanding the nuances of electrochemistry.

I am extremely thankful to my colleagues at the Laboratory for Advanced Healthcare Technologies, Dr. Geethanga deSilva, for his guided mentorship, technical feedback and inspiration, Dr. Matthew Giovanetti and Dr. Charles Zimmer for their invaluable technical support and help all along the course of this research. I would also like to thank Dr. Adam Hauke from Novel Devices Laboratory for helping me with the experimentation and validation of the prototypes of my research. I would also like to thank Dr. Raj Bhatnagar for his kind support and invaluable advices/conversations throughout the course of my graduate studies.

Most importantly, my heartfelt love and gratitude to my family for their unwavering confidence in my abilities and motivation. I will always be indebted to my parents, Aruna and Rakesh for the unconditional love and support at every step of my life. Their invaluable lessons and enthusiasm towards life have helped in shaping me into the person I am today. My loving and kind twin brothers, Garvit and Pulkit deserve all my gratitude, love and affection for being my strongest supporters for as long as I can remember. I would also like to acknowledge the encouragement and support I have received my dear friend Navneet. His technical contributions and unfaltering friendship has helped me continue my journey through every impediment.

I also extend my thanks to family and friends in Cincinnati for their constant support and fun times during my graduate studies. Their contribution has been immense in making the city a home away from home for me and making me feel loved and cared for always.

Lastly, I would also like the acknowledge the support from University of Cincinnati and the Department of Electrical Engineering and Computer Science and members of the faculty and staff for providing every level of support and help during the time of my graduate studies. I am thankful to Dorothy and Anthony Seta and all the other staff of the Department for their kind support and help in the departmental activities. I am also thankful to Ms. Julie Muenchen for being available always as a beacon of support and strong leadership for all graduate students in the college.

Table of Contents

List of Figures

List of Tables

List of Abbreviations

EIS   Electrochemical Impedance Spectroscopy

DSC   Digital Signal Controller

BIA   Bio-electrical Impedance Analysis

ADC   Analog-to-Digital Converter

DAC   Digital-to-Analog Converter

PLL   Phase Locked Loop

PWM   Pulse Width Modulation

LPF   Low Pass Filter

AAF   Anti-Aliasing Filter

DMA   Direct Memory Access

IVT   Interrupt Vector Table

UART   Universal Asynchronous Receiver Transmitter

ICD   In Circuit Debugger

PCB   Printed Circuit Board

FFT   Fast Fourier Transform

1.Introduction

1.1 Wearable bio sensing

Wearable biosensors are striving fast towards becoming ubiquitous devices that can closely monitor human activities. While many bio sensing strategies have been suggested, analysis of biofluids has shown promise as an approach that provides non-invasive access to relevant physiological biomarkers without significantly limiting the user activities of daily living. Therefore, an attractive research aim for many wearable devices is to enable real-time continuous gathering of physiological biomarker information from biofluids and thus enable monitoring of a user's health status and fitness prediction. At present, commercially available wearable devices are capable of only tracking an individual's physical activities. Unfortunately, they are not well suited to providing insight into biomarker detection and analyses of diseases. Because human sweat contains physiologically and metabolically rich physiologic information, measurement of biomarkers in human sweat could provide non-invasive access to important physiologic health data[1]. Sweat analysis is currently used for applications such as disease diagnosis, drug abuse detection, and athletic performance optimization[1]–[3].

To enable biomarker detection in biofluids, electroanalytical techniques have been developed including cyclic voltammetry and square wave voltammetry. However, these techniques are not well suited to integration into wearable applications because they are time consuming, require complex hardware and can be expensive to implement. Impedance analysis technology is well suited to meet these problems as it is more sensitive, simple to implement and cost effective which ultimately leads to systems that yield more complex information about these biomarkers with

inexpensive and wearable hardware[4]. If bio impedance analysis is performed on a spectrum of frequency, it reveals the frequency response of the system and is helpful for both diagnosis and characterization[5]. EIS methods can elucidate the electronic and physical properties of electrochemical systems including diffusion coefficients, adsorption mechanisms, capacitances, charge transfer resistance, and electron transfer rate constants. Due to its sufficient sensitivity, simplicity and cost effectiveness, it has been increasingly applied in bio sensing with numerous methods in the past few years[6], [7].

1.2 Applications of Bio Sensing in Healthcare

In today's healthcare landscape, there is a great need for multipurpose and reliable tools that aim to improve patient quality of life while reducing manufacturing costs[8]. Traditional diagnosis for prevention, identification, and treatment of diseases is time consuming as well as expensive and is being replaced by point of care technologies, promoting portability, rapid analysis response and low cost for the equipment. This approach is possible thanks to the technological miniaturization development in different fields, especially in the field of electronics. This progress combined with dramatic advances in connectivity and communication resources opens the door to new ubiquitous devices[9]. The medical field has greatly benefitted from the technique of EIS where it is called Bioelectrical Impedance Analysis (BIA) and is applied to the surface of the body. BIA is used to measure extracellular, intracellular, and total body water, as well as to monitor the changes in the amount of free fat mass in the body [10]. It has also been used for characterizing biological materials, which include lipid bilayers and many membrane proteins[11]. The most recent and perhaps most attractive medical application of EIS is its use in the monitoring and detection of biomarkers in biosensors as a function of frequency [12]. The technique involves the measurement

of system responses over wide bands of frequencies and eventually the evaluation of the impedance of the system. It has also become popular in health monitoring systems where it is used for specific analyte detection utilizing electrochemical sensors. When the changes at a surface level in an EIS test under specific parameters are characterized, it reveals a diagnostic application whereas tailoring of system parameters is required to obtain effects on the surface thereby revealing characterization application. Interestingly, EIS is a test that overpasses both purposes of diagnosis and characterization.

1.3 Research Motivation- Parallel Sensing

In our previous work[13]–[15], we focused on decentralization of diagnostic testing from large and expensive clinical laboratories to portable and low-cost alternatives. Even today, there is a scarcity of commercially available small form factor EIS systems intended for non-laboratory-based testing. There is also a great demand for electrochemical biosensor modules that are portable and able to provide more information and rapid response from the biological fluids. If a single device can provide more than one important piece of information by running one test or several tests simultaneously, this decreases the cost and time considerably. A multi-analyte testing point of care platform that is not complex, sensitive, specific and robust would be the best option to have as a point-of-care device. Multiplexing strategies can analyze multiple biomarkers concurrently and have been used for biomarker discovery. They demonstrate high specificity, low limits of detection and short analysis times. Most clinical applications of multiplexing devices include the diagnosis and prognosis of disorders such as cancer, diabetes and other communicable diseases [16]. Even though multiplexing is becoming increasingly important, the number of multi-analyte point of care devices is relatively few. Some devices have been reported that perform parallel

electrochemical bio sensing using different techniques such as cyclic voltammetry and immunoassays [16]–[19]. The main objective of this research is to enable development of medical device considering the following three in-demand techniques: wearable, biofluid of interest testing and impedance analyses. Combining these three powerful technologies can have significant improvements in advancement of wearable sensing technology. In addition, to being viable as a wearable health monitoring technology, the proposed technology must be lightweight, provide appropriate power management for a wearable device, enable biomarker detection in sweat and support impedance analyses techniques that are fast, label-free and sensitive using multi sensor.

1.4 Problem Statement

The overall objective of this research is to advance the contemporary portable EIS sweat biomarker analysis platform research for a sophisticated wireless platform that can perform more than one different EIS tests simultaneously. The requirement is to implement a demonstrative electronic platform that is appropriate for integration into a sweat patch that integrates more than one sensor. The device must also include an interface module with device for communication, power management circuitry and support the application of serving as a stand-alone medical device for biomarker detection. The modules interconnect with each other to be able to measure signals from multiple sensors in parallel (sequentially) and transfer them to the terminal via the communication platform. Understanding the mechanics of the platform, the physical characteristics of the sensors at hand and their behavior when they are connected in parallel to the system is important. There is a need to build into the application, the correlation between different sensors allowing users to run tests smoothly. These different EIS tests can then be multiplexed themselves to test a larger number of similar tests simultaneously. The problem statement has been formulated based on our

preliminary work where we developed a stand-alone single-frequency EIS module for one sensor [13]–[15]and ongoing research work on handheld impedance analyzers as reported in [20], [21] with prototype devices motivations as reported in [22], [23]. Our rationale is that integration of more than one sensor should provide us with validation of biomarker detection for the same samples drawn thereby confirming detection and sensitivity.

1.5 Thesis Outline

In this thesis, we present a compact microcontroller-based EIS system that allows measurement of impedance at frequencies up to 2.5 kHz. This frequency range is an acceptable range to extract information about body fluids and analytes.

Chapter 1 gives a brief introduction to the EIS technique and the application of the technique to the field of medical sciences. It also discusses in brief the motivation for a point-of-care platform and points out the main goals of the research work carried out.

Chapter 2 gives a brief history of the EIS process and its development through the last two or three decades. It also discusses the various applications that have benefitted from the technique of EIS and its applications in the field of medical devices.

Chapter 3 describes the requirements elicitations for the development of the complete product. All these requirements are not mandatory to be designed into the system but are recommended.

Chapter 4 describes in detail the design of the proposed system that generates signal for stimulus, calculates the magnitude and phase of impedance of a cell using software-based control over the microcontroller and peripherals thus reducing the system size. It also discusses the integration of the hardware and describes its functioning.

Chapter 5 discusses the experimental setup used to perform the experiments and the results obtained on the portable platform.

Chapter 6 summarizes the research, methods and integration work described in the thesis and discusses the opportunities for future work.

2. Literature Review

2.1 Review of EIS and its process

The Process of EIS

The most basic understanding of EIS is that it involves activating a given electrochemical cell with a potential and then measuring the response current flowing through the cell. The potential that is applied is an AC potential superimposed on a DC offset and the response is obtained as the current flowing in the cell as a result of the stimulus. The impedance of the cell is computed as Z = V/I, where V is the voltage and I is the current flowing through the cell. Since, impedance is a complex value, it can be broken down as Z= R + jX, and

$$|Z| = \sqrt{(R^2 + X^2)} \tag{1}$$

$$\theta = \tan^{-1}(\frac{X}{R}) \tag{2}$$

The electrochemical cells are known to exhibit complex behavior that cannot be represented by a single passive circuit element such as resistor. It shows active component characteristics that must be represented by complex impedance which is the ability to resist the flow of electric current without the limitations of Ohm's law[24]. Therefore, the characterization of electrochemical cell using impedance is ideal as it takes the phase difference between input voltage and output current into account and is composed of various resistors, capacitors and inductors.

The amplitude level of the trigger potential or evaluating electrochemical impedance is usually low. The electrochemical cells in real world are non-linear systems, however, by simple

linearization theory, it is understood that at small amplitudes of AC signal, they behave pseudo-linearly and do not exhibit harmonics at the excitation frequency as illustrated in Figure 2.1.
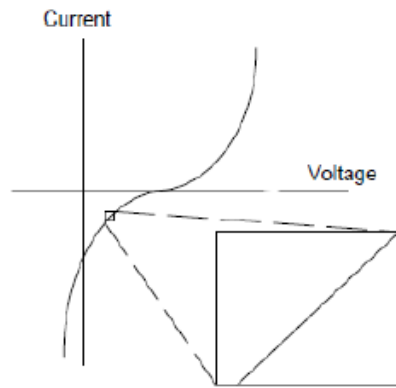
Figure 2-1 Illustration of pseudo-linearity of electrochemical cells

The characteristics of linear systems where the excitation signal and response signal both exhibit variations in amplitude in a linear fashion with visible phase shift as shown in Figure 2.2.
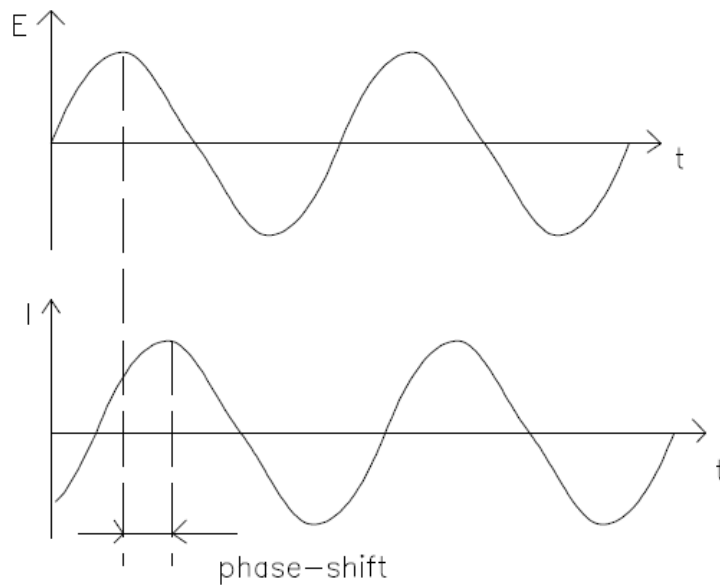
Figure 2-2 Sinusoidal Current Response in a Linear System [24]

The excitation signal can be expressed as a function of time and is given by

$$E_t = E_0 \sin(\omega t) \tag{3}$$

where E0 is the amplitude of the signal, Et is the voltage and ω is the frequency. In the linear system, the response signal It, depicts a phase shift and a different amplitude, I0.

$$I_t = I_0 \sin(\omega t + \emptyset) \tag{4}$$

The impedance of the system can be calculated analogous to Ohms law as given below in the equation where the impedance is given by a magnitude Z_0, and a phase shift, Ø.

$$Z = \frac{E_t}{I_t} = \frac{E_0 \sin(\omega t)}{I_0 \sin(\omega t + \emptyset)} = Z_0 \frac{\sin(\omega t)}{\sin(\omega t + \emptyset)} \tag{5}$$
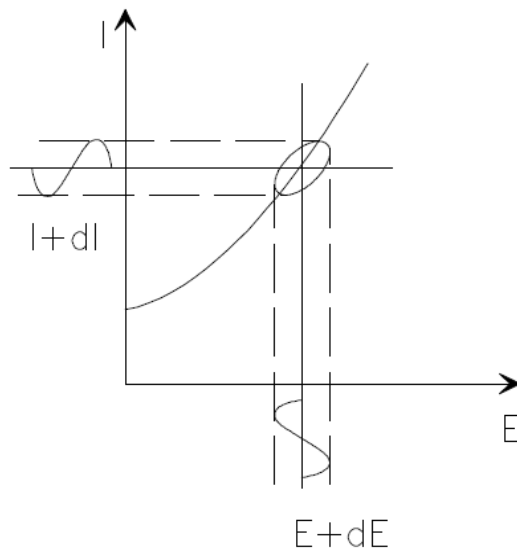
Figure 2-3 Illustration of the Lissajous Curve [24]

If the applied sinusoidal excitation signal is viewed against the received sinusoidal response signal, the resultant figure is an oval shaped curve called the Lissajous curve which is shown in Figure 2-3 above. It is one way of viewing EIS representations on oscilloscope screen before the modern EIS instrumentation was designed and the impedance is then given by the equation (4).

$$Z(\omega) = Z_0(cos\emptyset + j \sin \emptyset) \qquad (6)$$

The EIS measurements can be performed in a frequency range that can extend seven orders of magnitude or more from 10 mHz to 10 MHz [12]. The reason for collecting samples in a wide frequency range helps to obtain a good resolution of processes between the surfaces of electrode and provides with all the information needed to collect the bulk response of the material under measurement. The impedance measurement is usually carried out by using an electrochemical cell containing a solution that allows the measurement system to establish electrical connection with the coating[25].

2.1.2 Experimental Setup for EIS

The experimental setup for EIS typically consists on a potentiostat that provides the stimulus signal, an electrochemical cell and a signal processing module that determines the response of the system to determine the impedance[26][27].There are standard electrode configurations already known to us namely, two-electrode, three-electrode and four-electrode configurations. The substance to be investigated is usually applied on the electrode called the working electrode and the electrode used to balance the cell during the test is called the counter electrode. The choice of configuration generally depends on two attributes namely the drift potential of the counter electrode and the amount of current to be measured at the working electrode. Care must be taken to connect the electrochemical cell in the proper required configuration to avoid loss of valuable data. A two-electrode cell is mostly used for very low amounts of currents mainly in the range of pA to nA while a three-electrode cell is used for response currents in the range of uA or higher. A two-electrode cell is also used when exact control of the potential across the electrochemical cell is non-critical and when the counter electrode potential is expected not to drift over the course of

experiment. When the exact control of the potential across the electrochemical cell is critical, the three-electrode configuration is used in which the reference electrode accurately determines the potential within the electrochemical cell. This allows potential changes of working electrode to be measured as an independent of the changes that occur at the counter electrode, which is a clear advantage over the two-electrode setup. A four-electrode set up is also available which involves the addition of a working sense electrode but is seldom used in electrochemistry.

2.1.3 Measurement techniques

As mentioned in [28] the earlier measurement techniques involved in measuring impedance included the use of Wheatstone bridges and Lissajous technique. Other techniques such as the use of phase sensitive-detection with the use of Lock-in amplifiers is still very much in use. Most common is the use of Fourier analysis for determining the real and imaginary parts of the cell impedance. The experiment parameters and the settings of the potentiostats can be configured to obtain different EIS techniques such as potentiostatic, galvanostatatic, single-frequency and multiplexed EIS techniques. In this research work, we aim to develop the multi-sensor EIS tests for potentiostatic EIS capability.

2.1.4 Data Presentation

Since EIS is performed over such a wide range of frequencies, it generates a lot of data which is represented using the classic Nyquist and Bode plots. Bode plots help visualize the impedance data in terms of magnitude and phase angle as a function of frequency. Impedance has both real and imaginary components due to the capacitive and inductive components of the cell. If these imaginary components are plotted versus the real impedance of the cell, many important qualitative interpretations like charge-transfer resistance and solution resistance can be computed.

This plot is called the Nyquist plot and is advantageous than the Bode plot as it reveals better quality information while being complex at the same time. Because of its complexity, care must be taken to plot the data while keeping both the real and imaginary axes equal to avoid distorting the shape of the curve. The shape of the curve is important is revealing information like the charge-transfer resistance and solution resistances of electrochemical cells. Though Nyquist plot reveals more information as compared to Bode plot, it still has a small disadvantage of losing the frequency dimension of the data. A simple solution to this problem is labeling the frequencies on the curve which is not considered elegant. Because both Bode, and Nyquist plots have their own shortcomings, it is safe to represent one's data using both the plots.

2.1.5 Data Analysis using Equivalent Circuit Analogs

The electrochemical spectroscopy data once obtained from analyzing electrochemical cells then needs to be interpreted to understand the underlying characteristics. It becomes easier to predict the characteristics if these cells can be modeled as a network of passive electrical circuit elements. This network is called an equivalent circuit. The EIS response of an equivalent circuit can be calculated and compared to the actual EIS response of the cell. These models are applied to data obtained from the experiments and can be used to understand the system under various conditions. Capacitors, resistors and inductors generally known as passive elements are used to model the cells. Sometimes use of distributed elements takes place with the help of elements like constant phase element and Warburg impedance. The connections between these elements can be in series or in parallel.
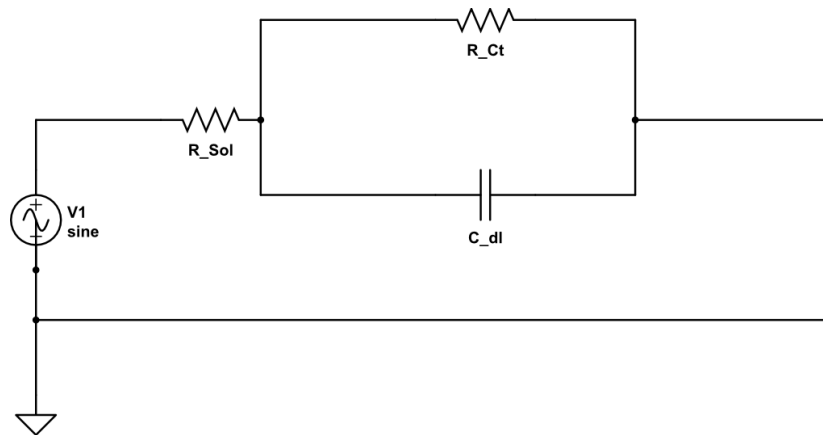
Figure 2-4 A circuit representing Randles Cell

Equivalent Circuit models represent the real world electrochemical cells in terms of resistances, impedances and capacitances[29][25][30]. Equivalent circuit modelling is a useful way to understand the mechanisms or processes involved in an electrochemical cell. Because a system's impedance at any frequency will often be dependent on more than one element of the cell, equivalent circuit modelling can help to separate out the contributions from each of the elements. This can help to understand the various things happening inside the cell in mechanistic terms. In equivalent circuit analogs, the resistors represent conductive pathways for ions and electron transfer. The capacitors and inductors represent the space charge polarization regions such as the electrochemical double layer, and adsorption/desorption processes at an electrode respectively[31].The cell model called the Randles cell, as shown in Figure 2-4 is one of the most well-known cell models. It is composed of a solution resistance (R_{sol}), a double layer capacitor (C_{dl}) and a charge transfer (R_{ct}) (or polarization resistance). The double layer capacitance is often in parallel to the charge transfer resistance.

2.3 Previous work on applications of EIS in medical field

Since its discovery, EIS has been applied in various fields for materials characterization and for the study of batteries, fuel cells, coatings and corrosion phenomena. The medical industry has benefitted with the development of biosensors that detect biomarkers in body fluids using EIS detection technique amongst others. One of the oldest application of EIS was in protein bio sensing where the high sensitivity of the technique established it as a label-free and wash-free detection method for a wide range of molecular interactions at the electrode surface. Such features are quintessential characteristics in a point-of care applications where it is necessary to reduce the number of assay steps, time and regents[2].Noninvasive measurements are a fundamental component of the process of diagnosis and bio sensing[1].

EIS has also been proposed as a simple, non-invasive technique to monitor the amount of fat and liquids in the human body. This technique is called as bioelectrical impedance analysis (BIA) which uses multi-frequency impedance analysis in applications like breast cancer screening[4], diagnosis of metallic prosthesis osseointegration[32].

The method provides unique advantages compared to other electrochemical methods, such as high sensitivity, signal quantification ease, and ability to separate the surface binding evens from the solution impedance. Impedance data are recorded in the range of frequencies, using AC of small amplitude. Compared to other electrochemical methods such as Cyclic Voltammetry or differential pulse voltammetry, which are also used to characterize molecular interactions on the surface of electrodes, AC impedance is less destructive to the measured biological interactions because it is performed in a very narrow range of small potentials. However, high sensitivity of the method

results in potential drawbacks which must be taken into account to obtain reliable and reproducible data [10].

While EIS is widely used in health monitoring systems for detection of specific analytes, the full potential of EIS is yet to be realized, partly because it is regarded as a specialty technique requiring expensive equipment. Furthermore, the large size of existing EIS equipment makes it difficult to integrate such techniques into small form factor systems that are hand held, wearable and intended for use in point of care testing. Thus, miniaturized and low cost EIS modules are needed to render effective point of care testing for biomarkers from electrochemical sensors.

2.3.1 Commercially available instrumentation

As mentioned earlier, EIS is universally applied in the field of health monitoring and medical device research. But EIS is a technique that employs expensive benchtop equipment running on high end software and sophisticated user interface for easier connection of the electrochemical cell to the hardware. Occasionally, EIS tests are also performed on samples located outside laboratories in the field. One of the many commercial EIS systems available is manufactured by Gamry Instruments, USA as shown in Figure 2.5(a). Their products such as the Reference 600^{TM} Potentiostat [33] are equipped to perform EIS from high impedance coatings to low impedance supercapacitors. They can handle 2, 3 and 4 electrode measurements, interfaces with lab computer and weighs about 7kg.

One other widely available commercial EIS system is developed by Metrohm called Autolab PGSTAT302N[34] shown in Figure 2-5 (b) that are capable of performing both single frequency and multi frequency EIS measurements. They have also been working on portable potentiostats

called the mini-series marketed as Autolab PGSTAT204 [34]for simple and entry level electro-analytical techniques, fuel cells, solar cells etc. Some electronics printed circuit board of the Benchtop Autolab Potentiostat is shown in Figure 2-5 (c).

(a)

(b)

(c)
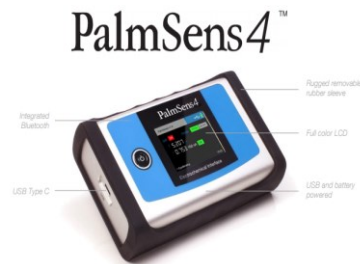
(d)

Figure 2-5 This figure shows the pictures of commercially available benchtop and portable EIS analyzers. (a) Benchtop Reference Potentiostat 3000 from Gamry Instruments [33], (b) Benchtop Autolab Potentiostat from Metroohm [34] (c) The complex electronics printed circuit board of the Benchtop Autolab Potentiostat from Metroohm [34] (d) Hand-held Impedance Spectroscopy equipment enabling multiplexed EIS from Palmsens[35]

Recent developments have seen the addition of PalmSens 4[TM][35], a commercially available device that is a portable impedance analyzer and can perform up to 8 or 16 multiplexed EIS tests simultaneously. As shown in Figure 2-5 (d), it is wirelessly connected with the help of a low energy Bluetooth module and is connected to a smartphone application that controls the test parameters and visualizes the test results. Recently, developments have been performed on realization of

portable impedance analyzer AD5933 from Analog Devices USA which has resulted in certain research prototypes presented in [36][37][38].

2.3.2. Research Devices

A potentiostat amplifier is a useful tool in many fields where electrochemical measurements are used. The electronics instrumentation, based on 3 electrodes configuration, is very useful in a wide variety of applications where different electrochemical techniques are used, from typical DC techniques such as amperometry, cyclic voltammetry, chrono-amperometry, pulse voltammetry etc., to AC techniques, such as EIS. Two different approaches can be followed in the design and implementation of a potentiostat amplifier: a discrete or integrated solution. Currently available commercial EIS platforms commonly use off chip signal generation techniques that make the system bulky [6-7]. Research prototypes of portable EIS suffer from long measurement times at the interface to the sensor [1].

Over the last decade, on-chip EIS measurement platforms have gained quite a lot of research attention and several research groups have been focusing on the development of such platforms. But demand for increased functionality, reduced system size, reduced size of the electrodes, defining complex arrays of sensors, ultra-low current detection and versatility, are introducing a major interest in advanced CMOS processes. A CMOS-based EIS system extract magnitude and phase information using in-phase and quadrature mixtures that increases the measurement times due to time required for low pass filters to settle [4]. This system as shown in Figure 2-6 (a) extracts magnitude and phase information using a seven-parameter sine fitting algorithm which is faster but requires a lot of processing at the signal processing end [6].

In the work presented in [39] as shown in Figure 2-6 (b), a feedback system calculates the impedance of a circuit under test using a peak detector external circuit which increases the measurement times to milliseconds for each iteration. Here, a trans-impedance amplifier (TIA) based architecture is used to calculate the magnitude of the signal that limits high frequency ranges due to comparator delays. Other EIS prototypes, implement external phase detector circuits to extract the phase information and heavily reduce the measuring range and adds hardware overhead [9].

In [40], a time domain EIS integration method where the sinusoid stimulus is generated using and external DAC has been reported. This microsystem was also implemented in a CMOS technology and in the low frequency ranges of 0.1 Hz – 10 kHz. Recent developments [20] in portable EIS systems include Arduino-based circuits that take advantage of ADC and DAC and employ a logarithmic amplifier to extend the impedance measuring ranges. The utilization of logarithmic amplifier at the front end has also been reported in [21] for impedance measurements in frequency ranges of 1mHz-100kHz. The system also employs a commercially available Arduino Duo board for data acquisitions and processing. Both these prototypes claim to be low-cost and portable EIS systems with uncertainty of below 5% of amplitude and phase.

The most recent research in EIS systems is the development of a wireless, stand-alone portable system that can transfer data to a terminal or a smartphone. A portable battery powered microfluidic impedance cytometer with a smartphone is seen in [40][22][23]. Developments of new ADCs or Impedance to Digital Converter (IDC) as they are called have been seen in [41] and [42] that propose to eliminate the conventional ADC usage in such platforms. There are two types of IDCs that this research group has been working on. The first one converts the real and imaginary parts of

the impedance into digital codes [42] while the second one converts the magnitudes and phases of

impedance into digital codes directly [41]. One of the most interesting features, that can be easily

achieved with this kind of instrumentation along with wireless connectivity, is the development of

multi-bio-analysis or multi-parametric device by means of different electrode arrays. These arrays

can be used as a multi-purpose system becoming an extremely versatile tool making it feasible to

perform different electrochemical experiences at the same time with different chemical species. The

multi sensor or multi sensing techniques as shown in Figure 2-6 (c) have been seen in [43][17][18]

which is the main aim and research of the project.

(a) (b) (c)
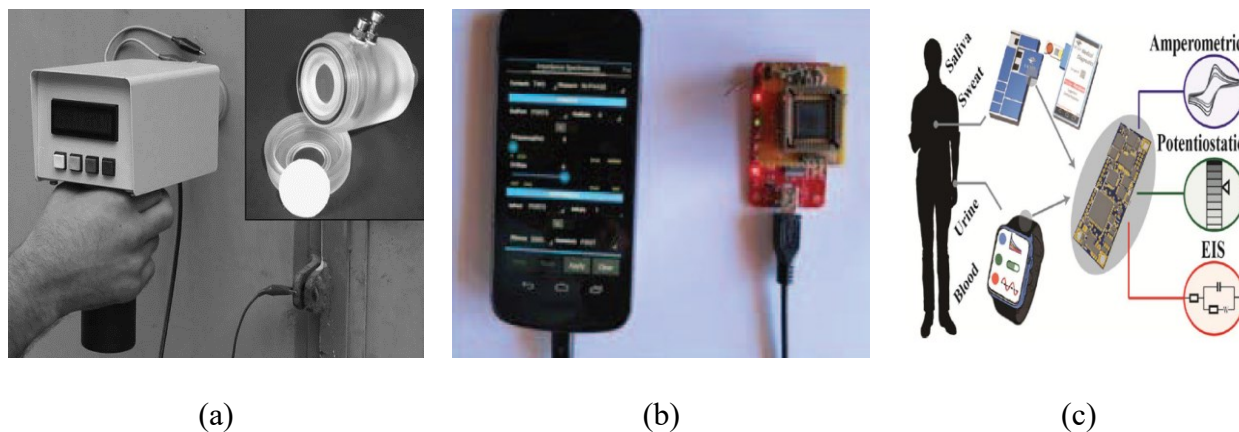
*Figure 2-6 This figure shows the pictures of research devices reported as impedance analyzers (a)
One of the first handheld EIS instrument reported by [12] in 2006. (b) Integration of smartphone
in the EIS instrumentation reported by[39] in 2014 (c) Multi technique equipment that can switch
between potentiostatic, galvanostatic and impedance spectroscopy measurements reported by [18]
in 2016.*

But these devices are not reported to show simultaneous EIS tests running on the same platform.

The device in [22] performs one sweat based glucose detection test at a time but can be configured

to run a different test for a different analyte with no change in hardware as long as the sensor is

based on the same technique. This device reports amperometric, potentiostatic and impedance

measurements that matched the performance of other platforms in terms of dynamic range, sensitivity and error but multi-sensor measurements have not been reported.

The ubiquitous availability of smartphone provides many excellent and easy-to-obtain functions in mobile way, such as touch-screen display, advanced computing capability, and powerful data storage, which has inspired a surge of peripheral apparatus linked to smartphones. A smartphone-controlled biosensor system with EIS has been reported in[44] to detect proteins for POC testing. The system is a hand-held EIS detector to convert bio-molecular interactions intro electrochemical changes and then transmit the impedance signals to smartphone by Bluetooth. This research work claims to be able to interface multiplexed interdigitated electrodes for EIS measurements, but no quantifiable results have been reported.

3. Research Objectives and Methodologies

The sweat sensing patch aims to measure multiple electrolytes, metabolites and other biomarkers at the same time. The different electrolytes and biomarkers will be measured with the help of respective analog sensors that are controlled using a high bandwidth microcontroller. The problem of the study is that the design of the sweat patch requires analog interfacing, digital signal processing (power consumption optimization) and algorithms needed to analyze the raw electrical measurements of biomarkers in sweat. Since this is a product developmental project, the problem at hand has been broken down into specific design aims as key steps towards achieving this goal.

Specific Aim 1: Design and implement an embedded system of hardware/software necessary to perform EIS measurements interfacing two sensors and performing signal generation and analog interfacing of the sensors with the microcontroller.

Specific Aim 2: Enabling wireless communication methods such as Bluetooth so that the device communicates the sensor data to a monitoring platform.

Specific Aim 3: Development of a control/analysis platform with real-time impedance data plotting for EIS data representation. By completion of this aim, the user will be able to input the test conditions for the sample to be tested and view the results on the platform.

3.2 Research Objectives

The medical device development process has become increasingly complex in recent years. The study suggests that stage gate processes are the predominant development model used in the medical device industry. A stage-gate system divided the innovation process into a predetermined set of stages, separated by gates characterized by a set of criteria to be met before the product can

advance in the process. Each stage, in turn, is composed of several prescribed activities that are in many cases related and that can occur in parallel. The stage-gate process[45] includes the following five phases: (1) initiation-opportunity and risk analysis, (2) formulation – concept and feasibility, (3) design and development – verification and validation, (4) final validation-product launch preparation, and (5) product launch and post launch assessment. Since this is a design and developmental research, the stage-gate process up until the verification and validation of the device at hand is established is followed.
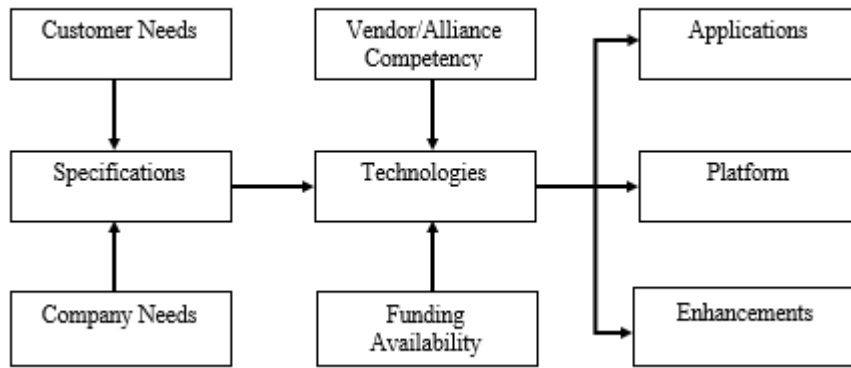
Figure 3-1 Block Diagram of requirements elicitation from the Stage-Gate Process

The Design Input and Product Definition Process as shown in Figure 3-1 is tackled first which allows the progression from specifications to available technologies and subsequent opportunities to define applications, platforms, and enhancements based on the developed technology concept. The complete specifications are identified and are explained in detail in the following sub-section.

1. Device Characteristics:

    ➢ The system must be portable,

- ➢ The system must be able to generate input stimuluses for all its test sensors using minimal external hardware,

- ➢ The system must be able to simultaneously sample all incoming data into the ADC to avoid losing important phase information,

- ➢ Since the sensors require different input conditions, there must be standby conditions for all sensors,

- ➢ The reference circuitry should provide a stable full-scale range equal to that of the input range of the ADC,

- ➢ The maximum current from the acquisition system, the MCU/DSP, wireless transmitter and all other attached peripherals shall not exceed the maximum output of the main power regulator,

- ➢ The system should have a mechanical on/off switch for full shutdown.

2. Technologies:

- ➢ Use of high speed processing unit for stimulus generation and response sampling is recommended,

- ➢ Use of wireless technology for communication is recommended,

- ➢ Use of scripting languages to response data is recommended,

3. Platform:

- ➢ The size of the system must be small,

- ➢ The system must be easily interfaceable to different types of electrochemical electrodes,

- ➢ The system should be capable of wirelessly transmitting all sampled data with no packet loss. The communication should be reliable and stable.

4. Enhancements:

  ➢ The system must have an interface to allow information exchange between user and device,

  ➢ The user must be able to enter important parametric information before the start of the tests,

  ➢ The User Interface must have a method for connecting and disconnecting the device,

  ➢ The User Interface must retrieve and present calculated data as well as review it.

4.System Design and Development

4.1 System Level Block Diagram

As per the requirements and specifications of the design, the system is required to run multiple EIS tests in parallel. This in turn requires the generation of multiple EIS stimulus signals, collection of their responses from the electrochemical cells and finally processing the data to yield the overall impedance value of the electrochemical cells under test. The overall design of the system is divided into various modules namely power management, stimulus signal generator, the analog front and back end circuitry, Bluetooth Low Energy transceiver, user interface, and the electrochemical cell or electrode connection configurations. The system is built around the dsPIC33F microcontroller from Microchip Inc. that generates the sinusoidal input stimuluses for the tests parallelly and digitizes the response current flowing across the cell thereby utilizing minimum power and external hardware circuitry. The analog interface circuitry assists in interfacing the electrochemical cells in test to the dsPIC33F and ensures there is no loss of response current signal during the entire test. The data collected is then sent wirelessly to a host PC via a Bluetooth Low Energy module. The PC receives the wireless transmitted data and saves it in a text file which is then processed to calculate the impedance values across the selected band of frequencies. A user-friendly interface helps the user to enter input conditions to run similar or slightly different tests on the sensors parallelly and displays the calculated impedance values in the form of Bode plots at the end of the tests. The hardware design for the proposed microcontroller-based prototype is as shown in Figure 4.1 and the modules are explained in detail in the following sections.
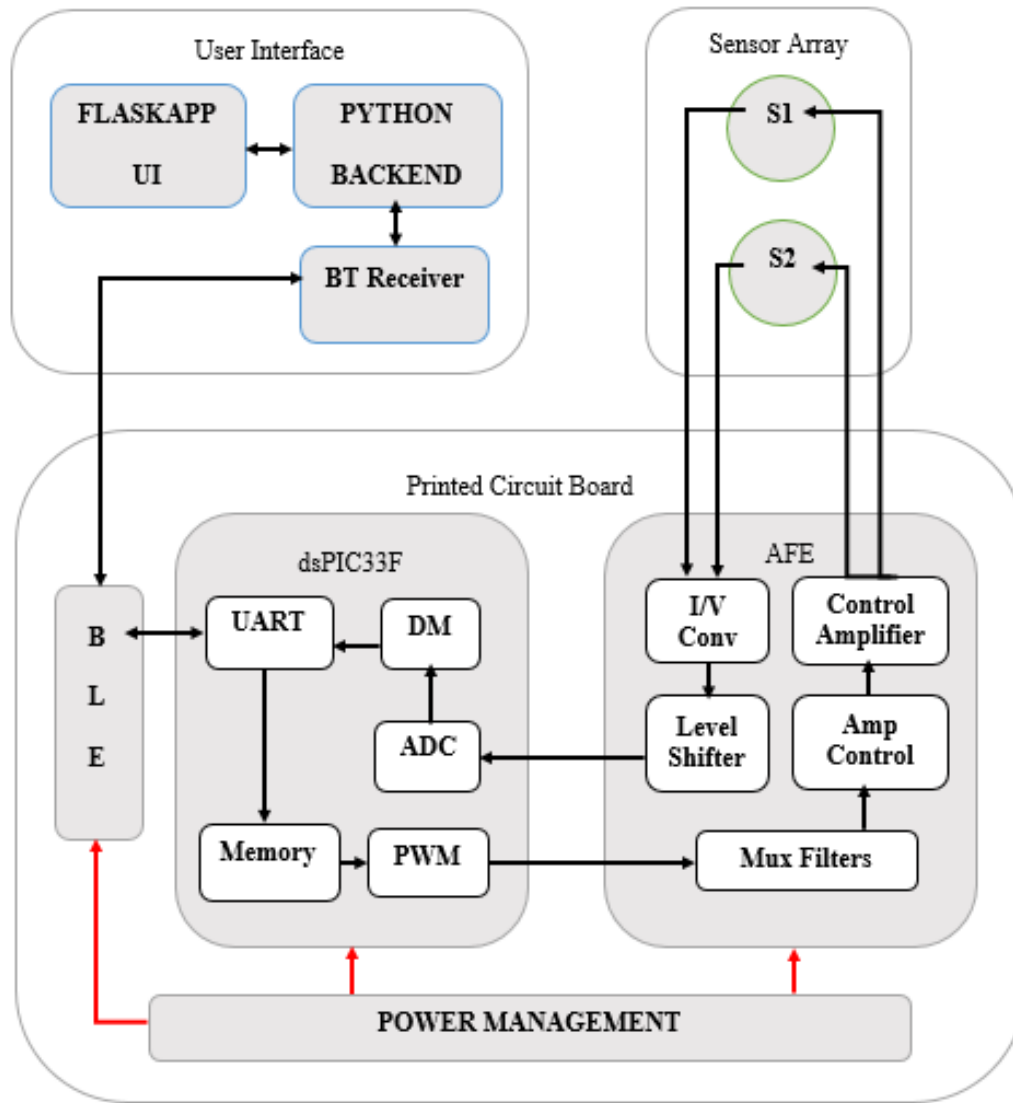
Figure 4-1 Block Diagram of the proposed EIS system

4.2 Power Management

The power management is responsible for powering the device from a wall adapter and generating

clean stable supply voltages. The board and all its peripherals require three different supply

voltages +3.3V, +5 V and -5V. Four ICs are used to generate these power sources using a wall adapter supplying 5V at 500mA power as shown in Figure 4-2. The 5V wall adapter is regulated using a LM117 regulator generating the positive 5V and 3.3V voltages required by the microcontroller and analog interface circuitry. The LM117 is a low-voltage, low-dropout regulator that can produce up to 800mA of current.
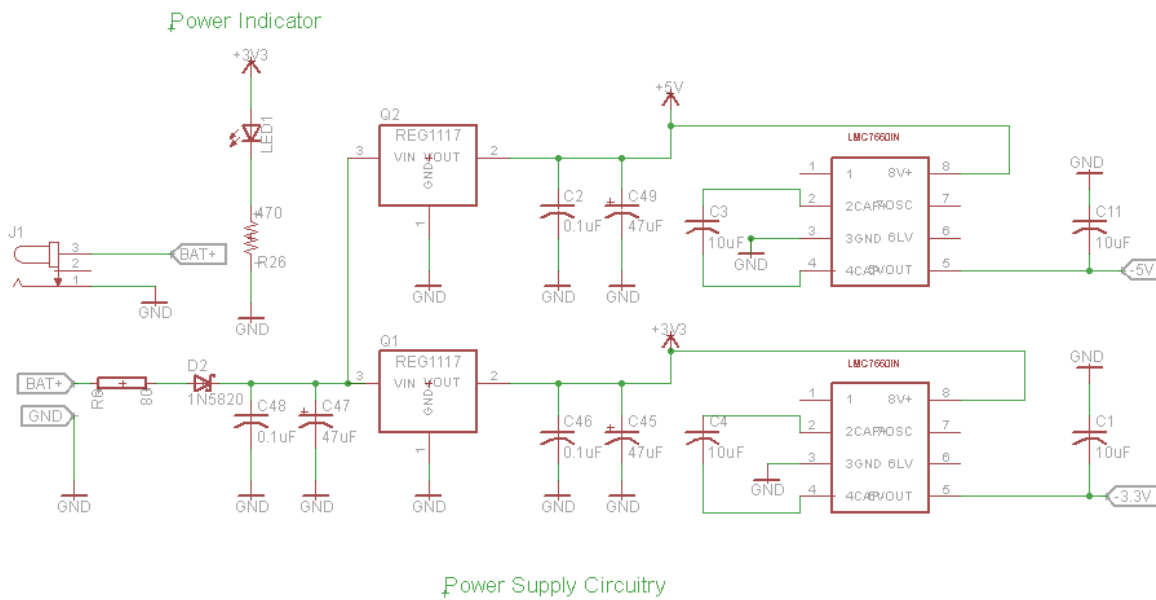
Figure 4-2 Complete power management circuitry of the proposed system

The negative 3.3 V is also put in the power management design in case any unforeseen changes in amplifier configurations lead to the requirement of negative voltage swings. Both negative supplies are devised using the positive +5V and +3.3V power supply and two LMC7660 voltage converters from Texas Instruments. The LMC7660 is a CMOS voltage converter capable of converting a positive voltage in the range of +1.5V to +10V to the corresponding -1.5V to -10V. It uses its built-in oscillator to switch 4 power MOS switches and charge two inexpensive electrolyte capacitors. The drive circuitry consumes little power and the power switches are matched and have

low resistance. The output is connected to a common power rail which supplies negative 5V and -3.3V supply to other devices. Although the LM117 regulators can supply clean voltages up to 800mA, an amount of 500 mA amperage is sufficient to power all the necessary circuitry on the board. Table shows the values of absolute maximum current consumption for all the devices on the board.

Table 1: Pin Description table for the dsPIC33FJ256GP710

Integrated Circuit or Device	Quantity	Maximum current consumption
dsPIC33F	1	250 mA
BLE112	1	26 mA
Op Amp – OPA380	2	20 mA (10 mA each)
Op Amp – TLE2064	2	50 mA (25 mA each)
Multiplexer-ADG680	2	40 mA (20 mA each)
Power Circuitry	3	~1 mA
LEDs	2	52 mA (26 mA each)
Total:		438 mA

4.3 Sensor and Equivalent Circuit Analog

As mentioned in Section 2.2.6 Equivalent Circuit Analogs are the representations of the real world electrochemical cells. The choice of the equivalent circuit model is critical to understand the characteristics of the electrochemical cells under investigation. Based on the literature survey, the most common choice of equivalent circuit model is dependent on the type of material to be characterized and the type of process being used. It is difficult to model an equivalent circuit for a electrochemical cell as it is likely to be unique to the sample under test. Computer algorithms are now available that can assign an electrical equivalent circuit to almost any impedance data given

to the computer. For this research work, the Randles Cell shown in Figure 4-3 is used with different values of resistors and capacitors to validate the system design and performance analysis.

4.4 Digital Signal Processor (DSP):

The control unit for the EIS platform is chosen from the dsPIC33F device family manufactured by Microchip Inc. that integrates the control features of a Microcontroller (MCU) with the computational capabilities of a Digital Signal Processor. It is a low-cost, high speed, 16-bit dsPIC
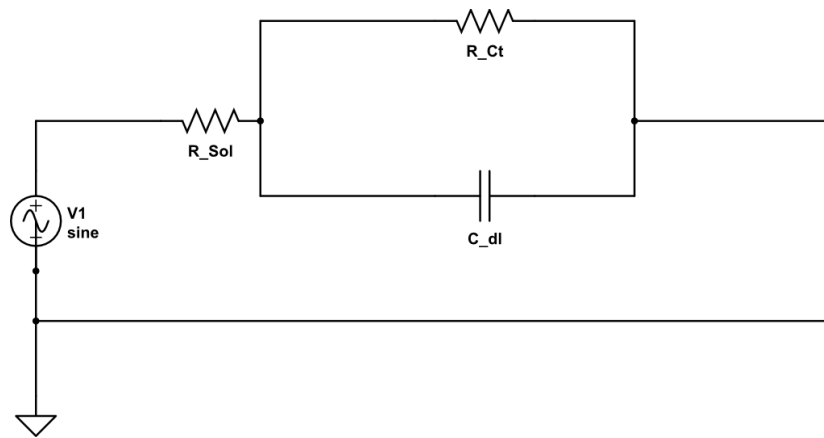
Figure 4-3 A circuit representing Randles Cell

microcontroller which consists of analog input and output ports, a communication module and is powered by a 3.3 V supply. The dsPIC microcontroller contains all the basic components which are required to arrange an EIS system except for the analog front end and these are the features that contributed to its selection as a part of the design and requirements mentioned in the Section 3.1. Specifically, it makes available the following important modules

- Low power consumption mode

- Flexible clock options ranging from external, crystal, internal RC to fully integrated PLL

- 64 KB of Data Memory and 256 KB of programmable flash memory

- A Pulse Width Modulation unit

- 3-wire SPI modules, I2C and Enhanced High-Speed Baud mode UART modules.

- A 10-bit, 1.1 Msps or 12-bit, 500 Ksps conversion Analog to Digital Converter (ADC) with 2,4 or 8 simultaneous sampling and 32 input channels with conversion in Sleep mode

The availability of the PWM module and ADC, and the synchronous operation of these modules permits to simultaneously carry out the generation of the sinusoidal stimulus and the coherent acquisition of the signals, making it possible to implement two algorithms to obtain the impedance from the samples of voltage and current In addition, the fast processing capabilities of the 16-bit microcontroller core allows one to perform in-line most of the operations required but the sine-fit thus reducing to a minimum amount of required RAM and the amount of data to be transferred to the PC. Two limitations still must be solved to successfully employ this device for bio-impedance measurements, i.e. the limited ADC sampling frequency and the wide range of impedances to be measured. The limited limitation connected to the ADC sampling frequency can be easily tackled thanks to the coherent sampling system which allows one to employ an equivalent-time sampling approach.

The controller with its DSP engine, 40-bit accumulators, hardware support for performing operations like divisions, barrel shifter, with 17 x 17 multiplier, large array of 16-bit working registers and a wide variety of data addressing modes, together provide the Central Processing Unit (CPU) with extensive mathematical processing capability. The DSP has flexible and deterministic interrupt handling, along with a powerful array of peripherals that renders the device suitable for applications requiring control. The process of EIS requires large amounts of data to be transferred between the peripherals and control unit. The Direct Memory Access (DMA) enables

overhead-free transfer of data between several peripherals and a dedicated DMA RAM. It also has a reliable, field programmable Flash program memory that ensures scalability of applications.

4.4.1 Pin Description

The DSP/dsPIC has 100 pins. Figure 4-4 illustrates the pin diagram of the microcontroller. Colored highlighting is used to indicate which pins are being used in for connections to the
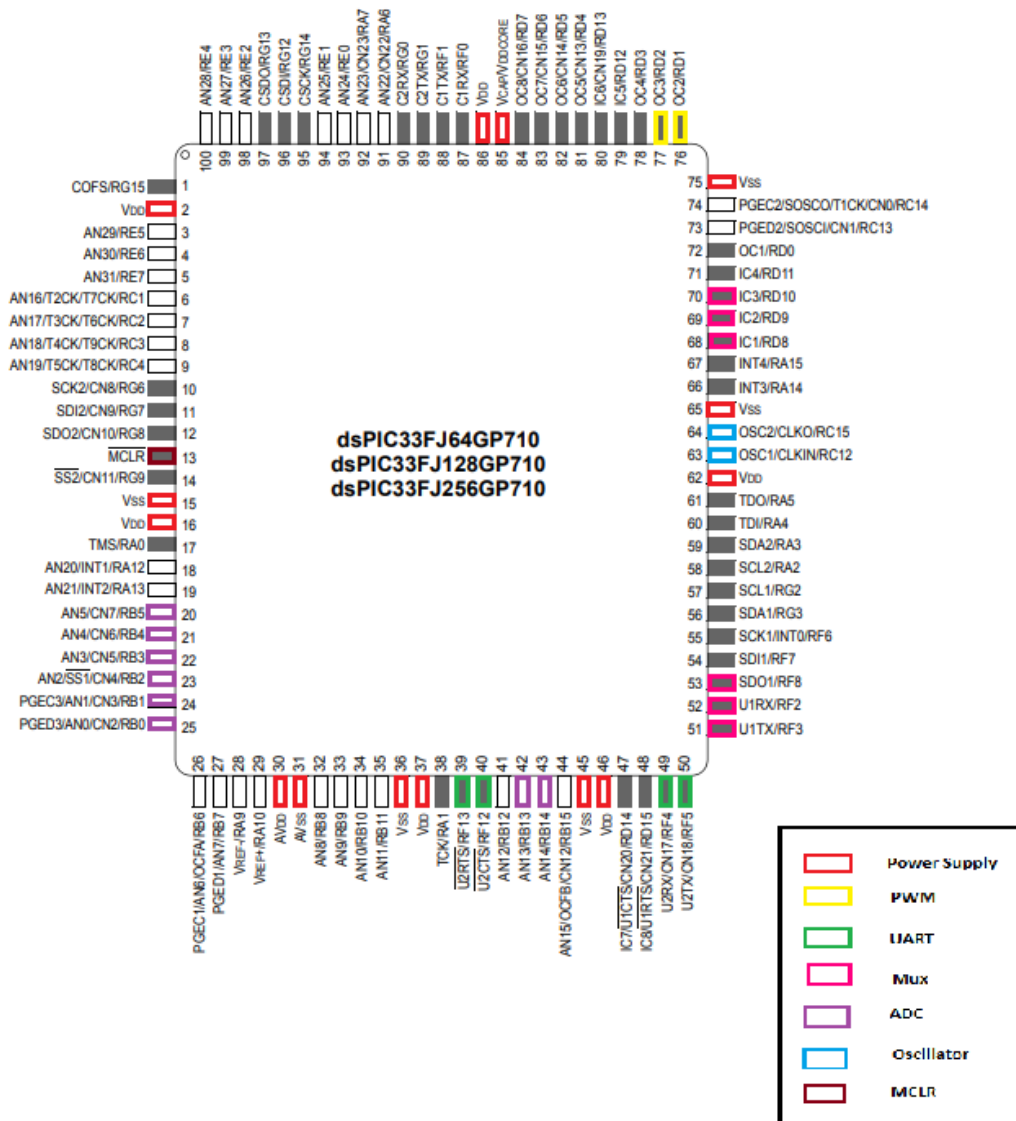
Figure 4-4 Pin Diagram of dsPIC33FJ256GP710 where color coding indicates the connections to various peripherals

corresponding peripherals. Table 1 lists the pins that are being used and provides a brief description

of the pin function.

Table 2: Pin Description table for the dsPIC33FJ256GP710

Pin Name	Pin No	Function	I/O	Description
OSC1/RC15/CLKIN	64	OSC1	I	Oscillator clock input
OSC2/RC12/CLKO	63	OSC2	I	Oscillator clock input
U2TX/CN18/RF5	50	U2TX	O	UART Data Transmit Pin
U2RX/CN17/RF4	49	U2RX	I	UART Data Receive Pin
U2RTS/RF13	39	U2RTS	O	UART Request to Send Pin
U2CTS/RF12	40	U2CTS	I	UART Clear to Send Pin
MCLR	13	MCLR	I	Memory clear input Pin
OC2/RD1	76	OC2	O	PWM signal generation Pin
OC3/RD2	77	OC3	O	PWM signal generation Pin
PGEC3/AN1/RB1	25	AN0	I	ADC input Pin
PGED3/AN0/RB0	24	AN1	I	ADC input Pin
AN2/SS1/CN4/RB2	23	AN2	I	ADC input Pin
AN3/CN5/RB3	22	AN3	I	ADC input Pin
AN4/CN6/RB4	21	AN4	I	ADC input Pin
AN5/CN7/RB5	20	AN5	I	ADC input Pin
AN13/RB13	42	AN13	I	ADC input Pin
AN14/RB14	43	AN14	I	ADC input Pin
IC3/RD10	70	RD10	O	To Multiplexer Pin
IC2/RD9	69	RD9	O	To Multiplexer Pin
IC1/RD8	68	RD8	O	To Multiplexer Pin
SDO1/RF8	53	RF8	O	To Multiplexer Pin
U1TX/RF3	51	RF3	O	To Multiplexer Pin
U1RX/RF2	52	RF2	O	To Multiplexer Pin

4.4.2 DSP Settings to get started

Power Supply Settings: All the VDD and VSS pins must be connected to the specific voltage power sources. This also includes the AVDD and AVSS pins regardless of whether or not the analog device features are used. The voltage for the core of this dsPIC33F is 2.5V and care must be taken to ensure that the voltage on the VCAP/VDDCORE pins is always regulated at 2.5V.

Decoupling Capacitors: The use of decoupling capacitors on every pair of power supply pins is required and a low ESR device with a value of 0.1 micro Farad is recommended. It is also recommended to place the capacitors on the same side of the board of the device and as close as possible to the power supply pins.

Serial Programming: Programming and debugging power pins must be maintained at 3.3V

Oscillator: There are many oscillator settings available on the dsPIC33F and for this application we choose to use an external 8MHz oscillator source which runs at 40MHz. This is because the instruction execution speed or device operating frequency (F_{CY}) up to 40MHz are supported by the dsPIC33F. It is connected between pins OSC1 and OSC2 and can be switched to a different frequency using programmable scalars.

Instruction execution speed or device operating frequency, F_{CY}, is given by

$$FCY = FOSC/2 \qquad (7)$$

For the primary oscillator with PLL mode, the PLL output F_{OSC} is given by

$$FOSC = FIN * (\frac{M}{N1 * N2}) \qquad (8)$$

where FIN is the frequency of the crystal oscillator = 8MHz in this case. M is a factor by which the input frequency to the VCO is multiplied to achieve PLL. N1 and N2 are prescale and postscale

factors and can be selected using special registers to achieve the desired frequency. Therefore, the device operating frequency can thus be calculated as

$$FCY = \frac{FOSC}{2} = \frac{1}{2}\left(\frac{FIN * M}{N1 * N2}\right) MIPS \qquad (9)$$

The design of oscillator is parallel cut crystal. The device uses 8 MHz 20 pF crystal. Capacitors C1 and C1 are 22pF ceramic capacitors.

Timers: In this application, timers are used with all modules such as PWM, ADC and even the DMA mainly for interrupt handling and it is imperative to set priorities to these timer interrupts to avoid non-sequential program flow errors.

Interrupts: The dsPIC33F's interrupts are managed by a smart interrupt controller which reduces the load on CPU by sending only a single interrupt request signal to the CPU for all the peripheral interrupt requests. The controller is aided by an Interrupt Vector Table (IVT) that has unique vector assignations for each of the 126 interrupts or exception sources. The management of interrupts is done by assigning priorities to them and organizing them in terms of their natural priorities while linking their position in the Interrupt Vector Table.

4.5 Signal Generation Module

As mentioned earlier, this research work aims to develop two different EIS tests on the same platform. This requires the development of two stimulus signals that can be modified to perform two similar or different tests simultaneously. We can recall that EIS is measured by applying a sinusoidal potential to an electrochemical cell and measuring the current response. The

requirements for an input sinusoidal signal to be applied to the cell are that it should be a constant amplitude ac signal with low amplitude and sweeping frequency within a designated range. Also, considering the device specifications, the requirement is to develop a small form factor EIS system. This means for every module development we must consider the elimination of extra hardware on the platform along power considerations. Out of the many sine wave synthesizers studied in literature requiring external chips and signal generators, we decide to make use of the powerful dsPIC at our disposal for generation of the entire two sinusoidal spectrums. The technique used is called Digital Design Synthesis and involves the use of the microcontroller along with low pass filters to generate a sine wave of any given frequency. The dsPIC consists of comparators and timers that can be used to design the stimulus generation and the concept and techniques are explained below.

4.5.1 Pulse Width Modulation (PWM) Module

The Pulse Width Modulated (PWM) signal is generated by utilizing the Output Compare (OC) module available on the dsPIC. The OC module has many operating modes, one of which is the PWM mode which is used to generate variable duty cycle. The duty cycle is generated by comparing the value of an associated timer with a comparison register and operation mode. When a match occurs between the comparison register and the timer output, the pin is toggled. This duty cycle of the PWM signal determines the amplitude of the sinusoidal signal at that point in its period. The PWM hardware block diagram is shown in Figure 4-5.
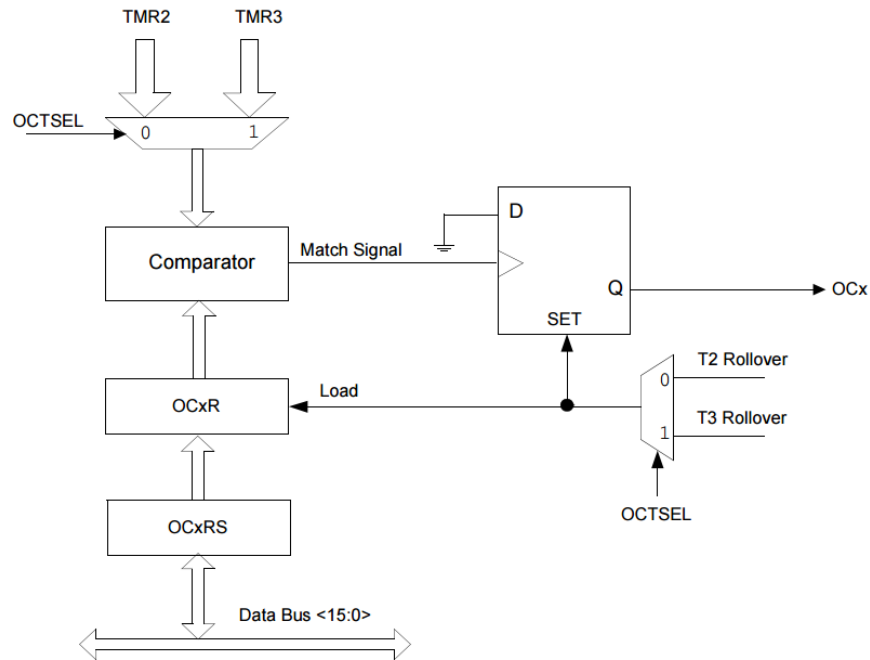
Figure 4-5 PWM hardware block diagram [37]

Working of the OC Module:

The PWM mode on the OC module is used to generate the variable duty cycle. This module is basically a comparator that compares the value between its primary and secondary compare registers OCxR and OCxRS. The Secondary Output Compare (OCxRS) register is used to specify

the PWM duty cycle and the initial PWM duty cycle is specified through the Primary (OCxR) register. A timer is used in conjunction with this module which when enabled, starts incrementing until it reaches the value specified in the period register PR. The timer loops from a value of '0' to a value equal to its period register and matches the contents of the OCxR (TMRy=OCxR) exactly once. When a match occurs, the OCx goes low and contents of the OCxRS are loaded into the OCxR. This loading of contents can be written any time, but it is latched when there is a Reset period match. This is important because if offers and extra space for PWM duty cycle that is a buffer and is important for smooth PWM operation.

The PWM period is written in to the PRy, the TMRy period register and is calculated using the following equation

$$PWM\ Period = \frac{1}{PWM\ Frequency} \quad (10)$$

$$= [(PRy) + 1] * TCY * (TMRy\ Prescale\ Value)$$

- If the duty cycle register has value of 0h, it is zero percent duty cycle (0% duty cycle)
- If the value is greater than PRy (Timer Period register), the OCx is high (100% duty cycle)

The PWM resolution depends on PWM frequency and the timer clock frequency and is given by the following equation

$$PWM\ Resolution(bits) = log_2\left(\frac{PWM\ Frequency}{Timer\ Clock\ Frequency}\right)bits \quad (11)$$

Generation of Sine Wave:

The concept explained above generates a PWM signal with a fixed duty cycle. For the generation of sine wave, the duty cycle needs to be modified every period and this is accomplished by enabling

the timer's interrupt to change the duty cycle at the end of each period. The entire sine wave is divided into certain number of amplitude divisions and each division is saved in the form of duty cycle value in a look-up table. This amplitude is determined in this application using an open source software that generates sine amplitude tables. At the end of each period a new duty cycle value is written into the OCxRS register and the process continues until the entire look-up table is read. A corresponding low pass filter is then used, and an analog voltage is obtained at the output that is proportional to the duty cycle and is given by the following equation

$$Vout = Vhigh * Dutycycle \qquad (12)$$

where Vhigh is voltage for logic HIGH for PWM pulse; in this case it is 3.3V.

A PWM pulse with 0% duty cycle is set to obtain the minimum amplitude and the one with 100% duty cycle is set to obtain the maximum amplitude of 3.3V in this case. Since the sine wave completes 360 degrees in one cycle the number of divisions corresponds to the resolution of the sine wave angle. Fascinatingly, these number of divisions control the maximum sine wave frequency to be generated by the module. The maximum sine wave frequency that can be generated with a pre-defined resolution value is given by the following equation

$$MAX\ Sine\ wave\ Frequency = \frac{PWM\ Frequency}{Resolution} \qquad (13)$$

For this dsPIC the maximum sine wave frequency that can be generated by the PWM method is

$$MAX\ Sine\ wave\ Frequency = \frac{PWM\ Frequency}{Resolution} \qquad (19)$$

$$= 1.25 \frac{MHz}{256}$$

$$= 4.8 kHz$$

Two different OC modules are used to generate the spectrum starting from 1Hz to 2.5 kHz with resolution of 256. The software can change both the magnitude and the resolution of the input signal generator. For simplicity, in this design only magnitude of sine wave can be changed. The look-up tables for these sine waves are saved in the memory of the dsPIC. The other option is to generate these look up table values rather than saving them but then the generation of the values must be faster than the requirement of the value for the PWM generation. In this test, 20 different frequencies are tested from 1Hz to 2.5 kHz.

4.5.3 Multiplexed Low Pass Filters

Once the PWM signal is generated, a low pass filter (LPF) is needed which is used as a Digital to Analog Converter for converting PWM into sine wave. This LPF blocks the high frequency PWM signal and lets the encoded low frequency sinusoidal waves to pass. To design this filter, the Cut-Off frequency or the corner frequency is to be decided. Four simple low pass RC filter with different cut off frequencies are designed and multiplexed using the following equation

$$Fc = \frac{1}{2 * \pi * R * C} Hz \tag{20}$$

Here the Time Constant $T_C = R*C$

The design tradeoff for this method is that the filter frequency must be chosen high enough to not alter the analog signal of interest. The step-size difference between the analog levels is dependent on the resolution of the PWM.

The passive RC filter is both simple and less expensive with its time constant τ being specified by RC and filter bandwidth by BW = 1/RC (rad/s). However, the stop-band roll of rate of the first order RC filter is a sluggish 20dB/decade, which causes the amplitude to decrease swiftly and exhibiting unsatisfactory performance in the PWM/DAC application This can be solved by various methods, one such being the use of active filters to avoid impedance loading issues experienced by passive filters. However, with active filters, one must also consider the gain bandwidth of the op-amps used. The input signal components with frequencies above the gain bandwidth will be attenuated since the op-amp will not have the ability to handle such frequencies.

With this as reference, the simple and easy solution to obtaining a sine wave is chosen which is
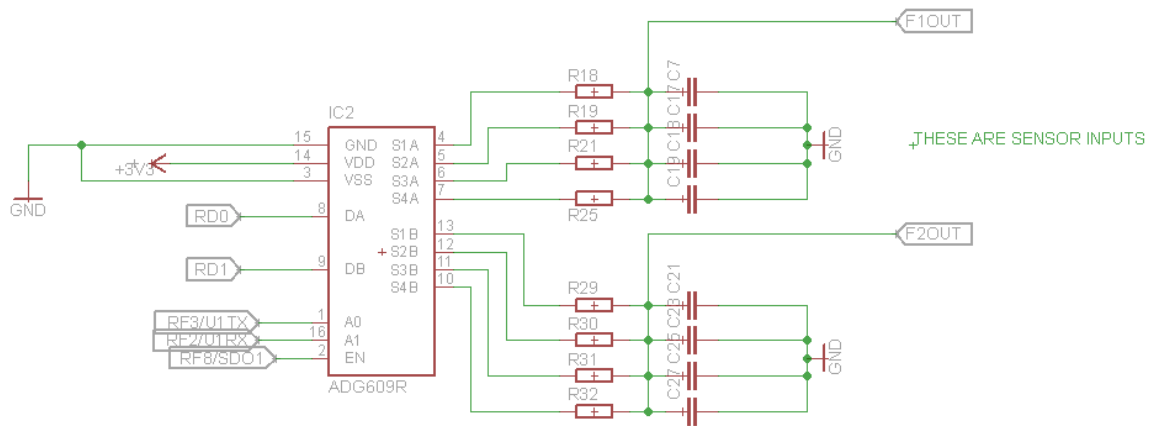
Figure 4-6 Circuitry for two channel multi-frequency sinusoidal input generation

the passive low pass filter and the results obtained are favorably suitable for the application.

Since, the low pass filters suffer from amplitude attenuation as they approach their cut-off frequency, there arises a need to switch to a different filter as frequency sweeps throughout the measurement. This is easily achieved by on-the-fly relaying a series of low pass filters as

frequency sweeps with the help of a multiplexer The multiplexer used is the simple 2x4 ADG609 [46] from Analog Devices and is controlled by two digital pins of the dsPIC33F. The ADG609 has two of these multiplexer devices and therefore can select four outputs for each input value thereby allowing filter control for both sensors simultaneously. The circuit schematic for this entire signal filter generation for two different sensors is shown in Figure 4-6.

The low pass filters as shown in Table 3 and as can be seen, their cut-off frequency is increased. Care is taken to maintain an optimum resistive value to maintain the input current flow and prevent the circuit from shorting. The capacitor value should not be so small that it falls prey to external and circuit noise. For this reason, a few RC combinations have been tested to ensure a properly filtered, noise-free signal is applied to the electrochemical cell.

Table 3 Low Pass Filter Component Values Used

Filter	Band Values	Cut-Off frequency	Component Values
LP Filter 1	10Hz	159.15 Hz	R = 10kΩ, C= 100nF
LP Filter 2	150 Hz	482.28 Hz	R = 3.3kΩ, C = 100nF
LP Filter 3	1000 Hz	7957.74 Hz	R = 200Ω, C = 100nF
LP Filter 4	10, 000 Hz	48228.77 Hz	R = 330Ω, C = 10nF

4.6 Analog Interface Module

In the entire design, the analog interface circuit is the most intricate and important module of all as it is the only medium that interfaces the three-electrode sensor or an equivalent circuit with the rest of the digital hardware. The key instrumentation of the analog interface module is the potentiometer, the main function of which is to maintain a constant voltage difference between the reference and the working electrodes. The main building blocks of the potentiometer are voltage divider and differential amplifier circuits that apply the sinusoidal stimulus generated from the microcontroller to the electrochemical cell. Other blocks include the circuity to measure anodic current at the working electrode as well as input and output filtering circuits.

Electrochemical cells can characterize the changes at the working electrode with respect to a reference electrode and the basic function of an analog interface module is maintain this potential at the reference electrode even with the application of input voltage. For this, an operational amplifier with large impedance is used that does not allow any current to flow to ground. The amplifier is connected to a virtual ground and the current from the working electrode is collected. A current to voltage converter using an amplifier, also called the transimpedance amplifier is then used to convert the current into voltage that is now readable by the microcontroller. Prior to being read by the microcontroller, the output voltage is fed into a level shifter to avoid any negative undershoots. This is done to ensure that the output voltage is compatible with the ADC of the microcontroller that can read only positive entities such as voltages. The output of the level shifter is then filtered through an anti-aliasing filter and then finally sent to ADC for digitization and processing.

4.5.1 Building blocks of Analog Interface Module

The analog interface module performs the tasks described above and to achieve these goals, the module is divided into smaller blocks as shown in Figure 4-7.

1. Amplitude Attenuator: This circuit is responsible to control the potential of the sinusoidal input to be in the order of a few hundred millivolts, preferably 50-200mV.

2. Control Amplifier: This circuit is designed for a three-electrode system which is responsible to control the difference between the two electrodes of the cell.
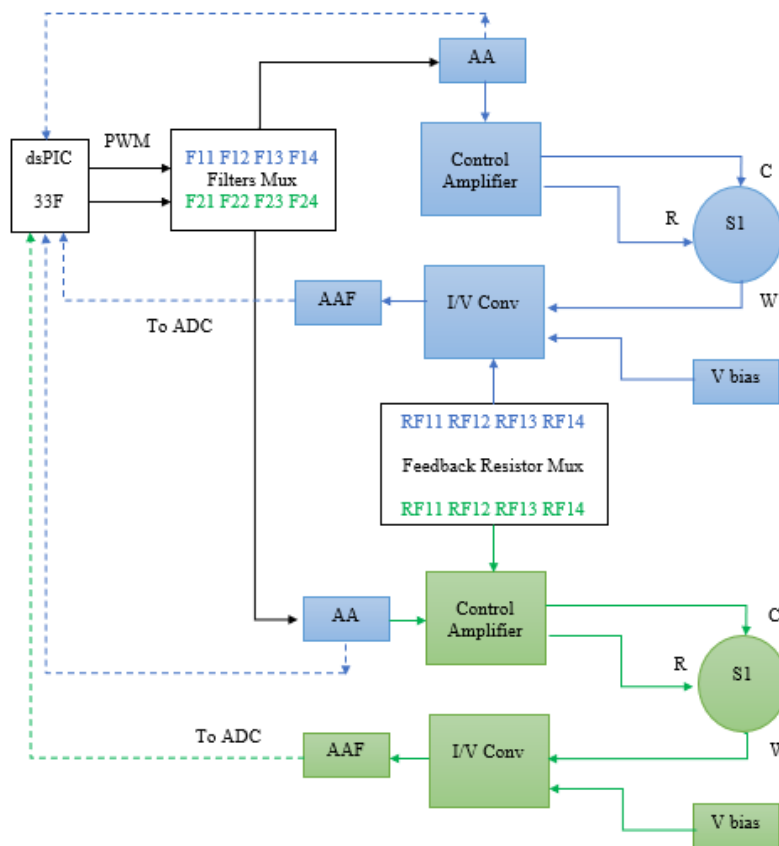

Figure 4-7 Block Diagram of the Analog Interface Module

3. <u>Transimpedance Amplifier:</u> This circuit is responsible to measure the current from the working electrode while maintaining the working electrode at virtual ground.

4. <u>Level Shifter</u>: This circuit is responsible to apply the bias voltage that shifts the non-inverting current output from the I/V converter to a positive value.

4.5.2 Amplitude Attenuator

The voltage generated from the PWM is a 3.3V signal and the requirement is a signal of a few millivolts. Using a simple resistor divider network to achieve such a large voltage drop is not advisable, therefore the amplitude attenuator for this deice has been chosen to a hardware-software combination. Also, having software control can enable the user to enter two different amplitudes for both the tests that are to be run parallelly. A non-inverting amplifier with a passive attenuator is used to decrease the amplitude of the input PWM signal. The amplifier's gain is set to be 0.1 and the amplitude of the sine wave is dropped down to 330mV from 3.3V. Then appropriate settings in the software are used to bring down the amplitude to the desired value. The range of amplitude that can be generated using this setting is between 0 to 330mV. In this configuration, an amplifier is used as an attenuator which means that the amplifier has less than unity gain (G<1). A few precautions must be taken when using amplifiers as attenuators. The first is to avoid using very large values of feedback resistances that can cause more system noise, larger offset voltages and can have implications on stability. Large feedback resistors along with amplifier's input and stray capacitance, can introduce a pole in the amplifiers feedback response, this causes additional phase shift, which reduces the amplifiers phase margin and can lead to instability.

4.5.3 Control Amplifier

This amplifier is used only for a three-electrode set-up. For two tests, two control amplifiers are used, and their purpose is to ensure that the cell potential V_{cell} tracks the applied sinusoidal potential without allowing any current to flow through the reference electrode (RE).

$$Vcell = -V_{RE} \qquad (141)$$

The voltage in the electrochemical cells is bound to change due to the reactions taking place in the cell. These changes in the cell should not be reflected on the reference electrode otherwise the current obtained from the working electrode is against a wrong reference. To avoid this, a feedback system employing an operational amplifier is used that maintains both the terminals at the same voltage. One terminal is connected to the reference electrode and the other is connected to the counter electrode. The voltage at these terminals must be equal, if it is not, the output of the op-amp changes until the potential becomes equal. Two TLE2062 low power- JFET-input operational amplifier from Texas Instruments is used to build the control amplifiers circuitry. The reason for using different amplifiers for both cells is to maintain signal and noise isolation between the two sensors. The chip has two operational amplifiers and features a high-output-drive circuit capable of driving 100-Ω loads at supplies as low as $\pm5V$. Because of extremely high input impedance and resulting low bias current requirements, the TLE2062[47] is well suited for low-level signal processing.

4.5.4 Transimpedance Amplifier (TIA)

The EIS procedure requires the application of a stimulus signal voltage to an electrochemical cell and the collection of the response current which is then divided by the stimulus voltage to obtain impedance of the cell. This response current if the current generated by the flow of electrochemical activity in the call and is measured with the help of a transimpedance. The basic circuit of a transimpedance amplifier is shown in Figure 4-8.
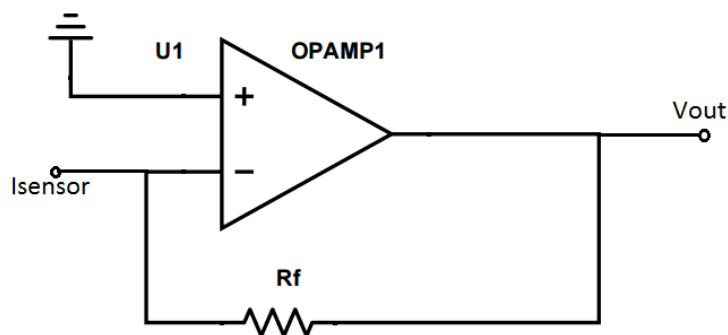
Figure 4-8 Basic circuit of transimpedance amplifier

Using an operational amplifier with good gain bandwidth and high slew rate, a current-to-voltage or transimpedance amplifier can be implemented. The OPA380 [48] transimpedance amplifier from Texas Instruments is chosen to convert the current response to voltage input for the microcontroller because it can also be used to amplify the very small current signal that is in the order of uA obtained from the cell. Some assumptions are made in the design of this circuit such that on application of a small sinusoidal potential, the electrochemical cell and the equivalent circuits are assumed to have linear behavior. For the application, the simplest form of amplifier is used which just has a feedback resistor, Rf. The gain of the amplifier is set by the feedback resistor

and this is connected to the inverting input of the operational amplifier which changes the value to –Rf. The voltage at the output of the operational amplifier is given by the equation

$$Vout = -Isensor * Rf + Vbias \qquad (22)$$

where, I_{sensor} is the current flow from the working electrode and V_{out} is the output voltage of the operational amplifier.

4.5.5 Bias Voltage Circuit

Once the current from the working electrode is converted to an analog voltage value, it needs to be digitized so that it can be read by the microcontroller. This operation is performed using the 10-bit ADC on the dsPIC33F on multiple channels. The microcontrollers is that they can read only positive signals and in the case of dsPIC33F, voltages between 0V and 3.3V can be measured. The analog current obtained from the working electrode is bound to consist of negative values, therefore, a bias voltage or level shifter circuit is designed using an operational amplifier to shift the analog output of the transimpedance amplifier above 0V. The output of the level shifter is then
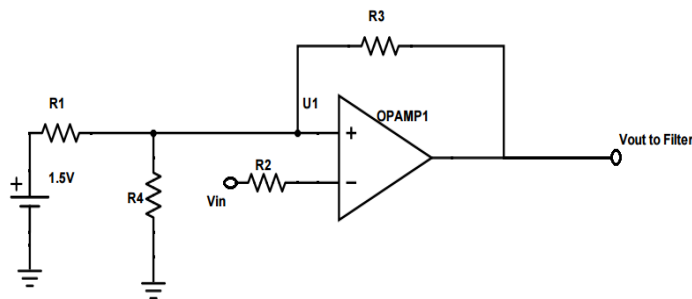
Figure 4-9 Bias voltage circuitry

connected to the ADC for digitization and further processing by software to convert the voltage back to current and calculate the impedance. Figure 4-9 shows the level shifter configuration.

One operational amplifier is used to build the transimpedance amplifier that converts the current response to voltage. Since this voltage response is negative for some frequencies and out of phase, a level shifter using the second operational amplifier is built to shift the voltage to above 0V to be able to be read by the ADC and to bring the voltage response in phase with respect to the input. The third operational amplifier on the chip is used to build an active anti-aliasing first order filter to which the voltage output from the level shifter is given as input. This output of this filter is then applied to the analog input of the microcontroller for digitization. A circuit level design of the analog interface module is shown in Figure 4-10.

Figure 4-10 Analog Interface Circuit

Figure 4-11 provides package level circuit diagram showing the usage of the four amplifiers on the chip to build the different blocks of analog interface circuitry.

Figure 4-11 Analog Interface built using the operational amplifier

4.2.7 Data acquisition and Analog-to-Digital Converter (ADC)

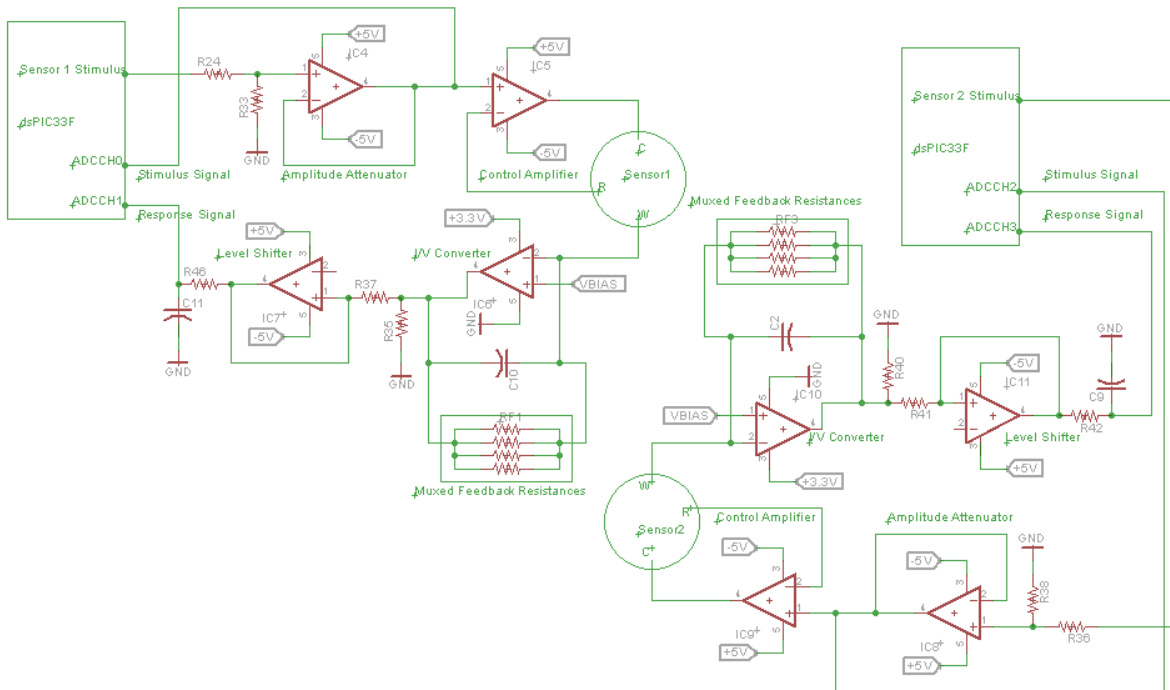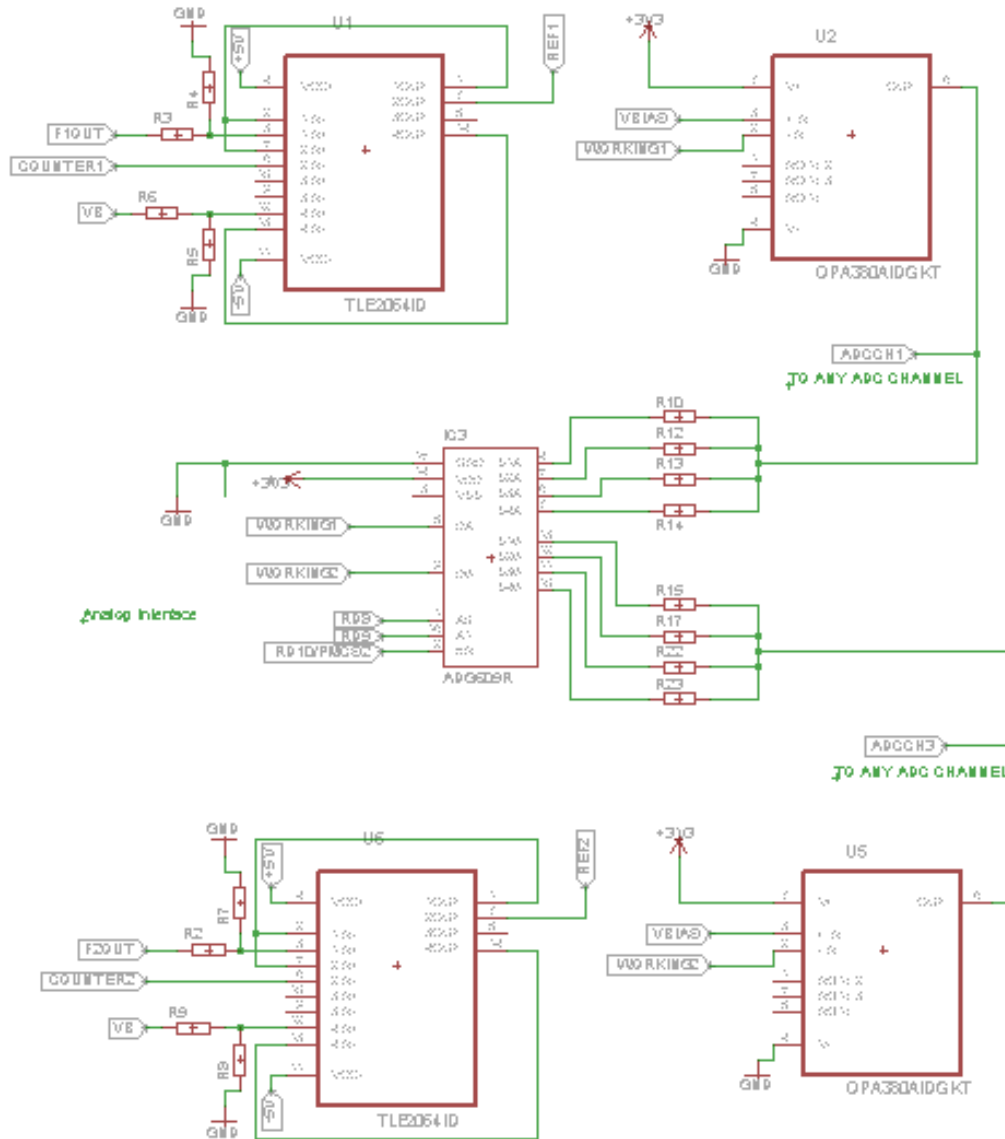Once the potentiostat is set up and is collecting the response current from the electrochemical cell, the next step is the acquisition of this response current as well as the stimulus voltage of both electrochemical cells. The digitized voltage and current values are then used to calculate the impedance of the cell. Since, the impedance calculations require the phase change values, it is imperative that both the stimulus and response signals are sampled simultaneously for correct phase change calculations. Since, we are running two different EIS tests and in an application, one can be used as counter, we have set up the system to sample response and stimulus signals from the cells simultaneously. The on-board Successive Approximation (SAR) Analog-to-Digital Converter (ADC) is used that is configured as a 10-bit, 4-channel, 500ksps data rate ADC. The onboard ADC hardware has four Sample and Hold (S&H) amplifiers that are unipolar and differential and therefore can easily sample up to four analog inputs simultaneously. It also has a multiplexer capability which enables up to 8 channels unipolar and 4 channels differential sampling simultaneously. Another efficient feature associated with the ADC of this dsPIC is the way data is stored after conversion. For this purpose, the microcontroller uses Direct Memory Access (DMA) which is a very efficient mechanism of moving data between Special Function Registers and variables stored in RAM, with minimum CPU intervention [49]. The DMA is equipped with a controller that can automatically copy entire blocks of data without the user software requiring to read or write registers every time a peripheral interrupt occurs. It works with a dedicated bus for data transfers and therefore, does not use the cycles of the CPU from the code execution[50]. The hardware of the ADC block has four sample and hold units, but it is equipped with only one conversion unit. This means that one can sample four channels simultaneously, but

conversion of these values happens sequentially as explained in the Figure 4-12 below. The
equations used for effective sampling and conversion times for these channels are explained below.

Channel No	Sample/Convert Sequence 1					Sample/Convert Sequence 2				
CH0 (S1 IP)	Sample AN0	Convert AN0				Sample AN0	Convert AN0			
CH1 (S1 OP)	Sample AN1		Convert AN1			Sample AN1		Convert AN1		
CH2 (S2 IP)	Sample AN2			Convert AN2		Sample AN2			Convert AN2	
CH3 (S2 OP)	Sample AN13				Convert AN3	Sample AN13				Convert An3
	◄———————— TSIM ————————►					◄———————— TSIM ————————►				

Figure 4-12 4-Channel Simultaneous Sampling

Calculation of Effective Conversion Time (TAD) for 4-Channel Simultaneous Sampling

According to the electrical characteristics of dsPIC33FJ256GP710 [51], the minimum effective
TAD is 70 ns and the minimum effective TSAMP is 1 TAD. At 40MIPS, TCY= 25ns. Since the
minimum TAD time is 70ns, 3 TCY would be 75ns, which is as close as possible to the minimum
effective conversion time. In the case of simultaneous sampling, since all four of the channels are
sampled together, for proper operation, it is imperative to wait for all channels to be converted
before sampling again. This total conversion time calculation is shown below

$$Min \ TAD = 70 \ ns \tag{23}$$

$$Min \ Sample \ Time \ (TSAMP) = 1 \ TAD \tag{154}$$

And it is already known that,

$$TCY = \frac{1}{40} MIPS = 25 \ ns \tag{25}$$

$$Min\ effective\ TAD\ in\ TCY\ (TADtcy) = \frac{70ns}{25ns} \tag{166}$$

$$= 3$$

$$Min\ eff\ TAD\ in\ ns = 3 * 25ns = 75\ ns \tag{177}$$

Now, for the platform, two channel CH0 and CH1 are being used for input and output respectively.

Therefore, maximum effective sample rate per channel is,

$$Maxm\ Eff\ \frac{Sample\ Rate}{Channel} = \frac{1}{Sample\ Time + Conversion\ time}$$

$$= \frac{1}{1TAD + (\#channels + 12TAD)} \tag{28}$$

$$= \frac{1}{1TAD + 48TAD} = \frac{1}{49TAD} = \frac{1}{49 * 75ns}$$

$$= 272.11\ kHZ$$

Finally, the value of conversion trigger source through Timer 3 is

$$PR3 = \frac{FCY}{272.11kHZ} = 148 \tag{29}$$

ADC Reference Voltage settings:

For normal ADC operation, the requirement of a stable reference voltage is imperative in order to have stable digital value converted from analog voltage. The reference voltage settings for ADC conversions are selected in the software and this voltage is supplied either internally or externally. The voltage reference high (VREFH) and voltage reference low (VREFL) in the ADC module is supplied internally by AVDD and AVSS pins while the external VREF+ and VREF- require certain specifications. For the EIS platform, internal voltage references of AVDD and AVSS are used since the internal voltage references are more stable. In this design, four channels are being

sampled simultaneously, 10-bit ADC is used and the conversion voltage appearing in the buffer is calculated as

$$ADC\ Voltage\ in\ mV = \left(\frac{Reference\ in\ mV}{1023}\right) * ADC\ Value \qquad (30)$$

In the system, reference value used is 3.3V. Given the 10-bit value it can be converted back to the analog input voltage as follows

$$ADC\ Voltage\ in\ mV = \left(\frac{3300}{1023}\right) * ADC\ Value \qquad (31)$$

4.6 Wireless Data Communication

After the data is acquired by the ADC, it is then bundled into packets and sent through a wireless communication system consisting of a low energy Bluetooth Module along with the Serial Communication interface available on the dsPIC. The dsPIC communicates with the BLE module via UART while paired with the device and sends data through traditional legacy serial communication methods. This is possible due to the Serial Port Profile implementation of the Bluetooth drivers, also known as the Cable Replacement Algorithm. The block diagram below in Figure 4-13 explains the entire two-way communication of the device.
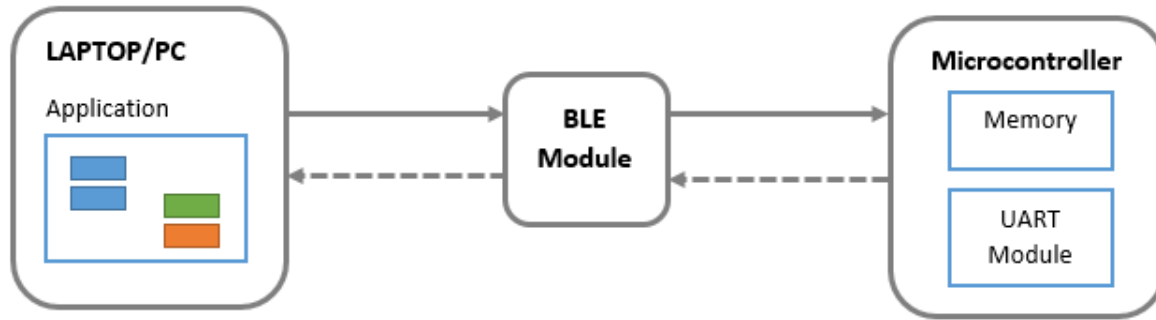
Figure 4-13 4-Wireless Communication Block Diagram

4.6.1 BLE

Due to the portability and compactness of the device, BLE module has been chosen for wireless communication which acts as a replacement for physical data buses. BLE has been developed to address the needs of new modern wireless applications such as ultra-low power consumption, fast connection times, reliability and security. It consumes much less power and can transmit data 50 times quicker than classical Bluetooth modules[52]. More information on BLE configuration is provided in Appendix 1. It integrates more than just the regular chipset in the module including the radio, software stack and GAT-based profiles. The bare minimum equipment is needed to program the BLE module which is the CC Debugger from Texas Instruments and the Bluegiga BLE112 itself. Along with the features mentioned above, what makes BLE the best choice for this project is the free software development possibilities provided by Bluegiga and the field upgradability of the firmware. The Bluegiga Smart Software enables developers to quickly and easily develop applications and edit it using flash memory. The Bluetooth Software Stack available consists of

1. BGScript^{TM} scripting language that allows us to write programs without using expensive hardware. It has its own syntax and examples of protocols along with BGScript syntax are available in the User Guides.

2. BGLib^{TM} lightweight host library which implements the protocol where separate host processor is used to interface to the BLE module over UART or USB. Since, our project is sending data to the BLE and BLE is just a wireless medium, we make use of the BGLib library to interface the BLE over UART.

3. Profile Toolkit^{TM} is a GATT based profile tool that enables software development quickly and easily to describe the BLE profiles, services and characteristics using simple XML templates. In the XML template, we specify the service and characteristic ID for the cable replacement module along with the desired baud rate and port settings.

In this device, the communication protocol is 8-bit, 1 stop, no parity and hardware flow control are used. After the hardware settings are written in the xml file and BGscript is sourced for cable replacement algorithm, the project is then compiled into a hex file and, then flashed onto the onboard CC2540 on the BLE112. The next step is to flash the newly compiled hex file on the BLE112. For this, we use the Texas Instruments SmartRF Flash Programmer by TI which is available free of cost. Once this has been done, we implement a Python script to read the data being sent to the Serial Port from the dsPIC via BLE module.

4.6.2 Data Transfer using UART

The dsPIC33F device has various serial and parallel communication modules and, in this application, the serial Universal Asynchronous Receiver Transmitter (UART) is used. The UART is a full duplex asynchronous system that is used to communicate with the peripheral, in this case,

a personal computer interface. The module is equipped with a hardware flow control option with the UxCTS and UxRTS pins and includes an IrDA encoder and decoder. The UART module includes a fully integrated Baud Rate Generator with 16-bit prescaler. Baud rates ranging from 1 Mbps to 12 bps at 16 MIPS can be achieved. A register BRGx is dedicated to UART module which controls the period of a free running 16-bit timer. The following equation shows the formula for computation of Baud Rate and the corresponding value that is to be written in the BRGx register for the desired Baud Rate. For this application, a Baud Rate of 9600 bps is desired and the corresponding value for the period register is calculated using the equation.

$$Baud\ Rate = \frac{FCY}{16 * (BRGx + 1)} \tag{32}$$

$$BRGx = \frac{FCY}{16 * Baud\ Rate} - 1 \tag{33}$$

Where F_{CY} denotes the instruction clock cycle frequency ($F_{OSC}/2$)

4.7 Data Processing Module

The data processing is done outside the printed circuit board module once the raw data is completely transmitted wirelessly. The raw data is saved into a text file on the PC and contains input and output sequences of 25 different sinusoidal waves contained in packets. There are start and stop commands that are transmitted at the start and end of the tests. As described in the data acquisition section, stimulus and response signals are sampled in such a way that only 200 samples are collected for each frequency. The complete period and number of samples in each period is pre-determined and thereby if the total number of samples are divided by the total number of frequencies sampled, it should yield the same 200 number of samples for each frequency. From

here the text file is read by a Python script that splits these sequences by identifying their delimiters and then two separate algorithms are run on each of the samples for both the tests thereby revealing the real impedance and phase change values. Before the data is collected by the ADC, it is passed through an anti-aliasing filter to eliminate high frequency interferences from the samples. In the following sub-sections, the anti-aliasing filters and the peak and phase detection algorithms are described.

4.7.1 Anti-Aliasing Filter (AAF)

To eliminate noise and high frequency interference from the sampled signal, an anti-aliasing filter (AAF) is implemented as shown in Figure 4-14.
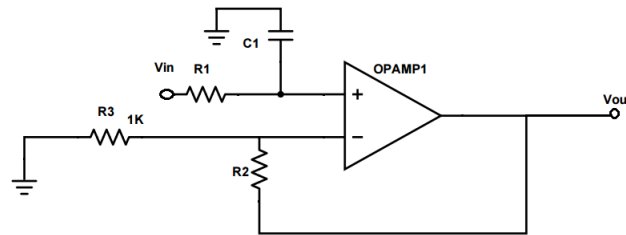
Figure 4-14 Anti-aliasing filter circuit

To design this filter, the Nyquist sampling theorem is followed which states that the sampling rate is required to be set at least twice of the maximum frequency component of the signal being filtered. This circuit is mainly incorporated into the design to eliminate interference, noise of stray signals that may be picked up by the ADC. These stray signals may interfere or alias with the required frequency range and sample data wrongly. The anti-aliasing filter attenuates the higher frequencies and prevents the interfered or aliasing components from being sampled by the ADC. At this stage, the anti-aliasing filter is an analog filter because the signal is still analog. Ideally, an

anti-pass filter should allow all the good frequencies to pass and cut off the undesirable frequencies. However, due to losses in the circuits and roll-off gains, such a filter is not totally realizable. An illustration of the filters is shown below in Figure 4-15.
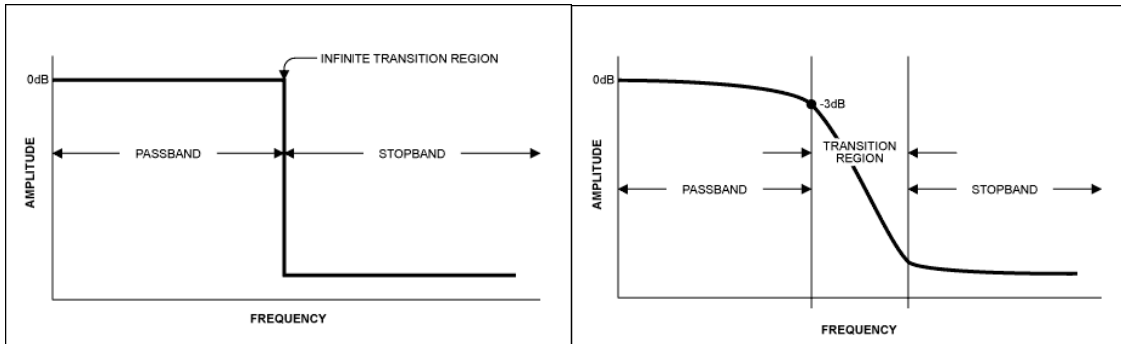

Figure 4-15 Ideal and Practical Anti-Alias Filter [43]

In the Figure 4-15 above, one filter is ideal that passed all frequencies below the cutoff and does not allow any frequency above it. The region where the signal can pass is known as transition band. In non-ideal filters which are realizable, some signals in the transition band can pass and cause interference. Therefore, the sampling frequency should always be calculated based on the greater than two times the highest frequency in the passband.

For example, it is required to sample a component of 20 kHz. The Nyquist theorem states a required sampling frequency of 40 kHz. The anti-aliasing has a cut-off frequency of 20 kHz, but since this is not an ideal filter usually the sampling frequency selected goes from 44 kHz to 96 kHz, which allows a transition band of at least 2 kHz. For this application, the highest frequency that is sampled is 20 kHz, therefore, the cut off frequency of the anti-aliasing filter is 20 kHz while, the sampling frequency is never less than 44 kHz.

4.7.2 Peak Detection

Once the stimulus signal is applied to the sample of interest and response signal collected, it is collected by the ADC of the dsPIC33F for calculation of impedance of the cell. This process of data analysis is done using the firmware. To calculate the impedance, the peak and phase of the samples are determined in the software. The peak to peak voltage of the sine wave is calculated by sampling at least one complete period and finding the maximum voltage value over the period. It is best to sample more than one period for each sine wave to calculate the peak to peak voltage for reliability. The negative voltage is offset using the level shifter and only the maximum and minimum voltages (in this case 0V) is to be subtracted to determine the peak-to-peak voltage of the sine waves. Two variables are used to perform this operation efficiently.

```
Function peakDetection( )
     max ← 0
     min ← 0
     peakValue ← 0

     for each ADCBufferValue in ADC_DMABuffer
          if waveAmplitudeValue > max then
          max ← waveAmplitudeValue
          end

          if waveAmplitudeValue < min then
               min ← waveAmplitudeValue
          end

     end

     peakValue ← max - min
     return peakValue

     end
```

Table 4 Pseudo-code for peak detection using which the peak-to-peak voltage of input reference and output response is calculated

Each sample in the text file is compared with the last sample until it reaches the total number of 200 samples. If the value of the current sample is higher than the last sample, its value is stored in a variable that holds the highest variable till now and the same is done to determine the smallest sample that is stored in a second variable. Finally, the two samples are subtracted to determine the peak-to-peak voltage. This peak-to-peak voltage is then converted into current and impedance values of the total cell are calculated. A pseudo-code for the peak to peak calculation is shown in Table 4.

4.7.3 Phase Detection

As discussed in section 2.2.1, the excitation signal is given by: $E_t = E_0 \sin(\omega t)$ and the response current is given by the equation: $I = I_0 \sin(\omega t + \emptyset)$. Therefore, the complex impedance can be calculated as

$$Z = \frac{E_t}{I_t} = \frac{E_0 \sin(\omega t)}{I_0 \sin(\omega t + \emptyset)} = Z_0 \frac{\sin(\omega t)}{\sin(\omega t + \emptyset)} \tag{34}$$

Phase difference between two sinusoidal signals can be calculated in the digital world using a microcontroller's memory and timing modules. The phase difference between two sinusoidal waves is usually calculated by evaluating the time when the signals cross zeros to get the time delay, also known as zero crossing evaluation. Most microcontrollers have hardware that allows a timer to run based on some internal or external trigger. If the timer is allowed to turn on when the first signal crosses the zero and to stop when the second signal crosses the zero time, the difference between the timer's on and off time gives the time between the zero crossings. The difference between the zero crossings of the signals gives the period. The phase shift in units of time is then just the time difference between the two signals divided by the period of the signal. The dsPIC has an Input Capture module based on timers that can be used to capture the signal's

zero crossings. However, since in this research work, an ADC is already employed to calculate the amplitude and the data is transmitted to the terminal via BLE, the phase difference is calculated without using capture timers.

For most EIS tests, the amplitude of the sinusoidal stimulus is usually contained to a few millivolts. After the current is collected from the sensors, both the stimulus and the response signals are level shifted by adding offset to the other half. This helps in the response being captured by the ADC since it accepts only values about 0V. The method of zero crossing or peak crossing is then applied to the samples collected and time difference between the two peaks of the waves or the two smallest samples between the waves is calculated. This processing is done off the chip after the data has been wirelessly transferred to the laptop. If the sampling frequency of the ADC is known, the samples can be converted into time and the difference between the two zeros be calculated. If the time delay is t, and the period of the sine wave is T, then

$$\frac{t}{T} = \frac{\emptyset}{360} \tag{18}$$

The phase 'Ø' is in degrees. The way to determine the lag and lead in the phase, if 't' is negative, the output lags the input and if it is positive, the output leads the input. A simple algorithm which is shown in Table 5 is used to determine the time difference between the maximum value of both the peaks. This time difference is then applied to the above equation to calculate the phase difference in degrees between the input signal and output response. The algorithm calculates the phase angles of all the frequencies measured simultaneously for all the sensors connected. The data collection is done in real-time by the UART and BLE chip and only the impedance calculations are done once the test is complete.

```
Function calculatePhaseDifference (timePeriod)
      inputMinIndex ← 0 outputMinIndex ← 0
      outputStartIndex ← 0 outputEndIndex ← outputWaveValueslength-1
      outputMinValue ← MAX_VALUE index ← 0    j←0

      for each ADCInputValue in ADCInBuffer
            if inputWaveValues[inputMinIndex]>inputWaveValues[index]
      then
                  index ← index+1
      end
      if inputMinIndex-timePeriod>0 then
            outputStartIndex = inputMinIndex-timePeriod;
      end
      if inputMinIndex+timePeriod<outputEndIndex then
            outputEndIndex = inputMinIndex+timePeriod
      end
      for each ADCOutputValue in ADCOutuffer
            if outputMinValue>outputWaveValues[j] then
                  inputMinIndex ← i
                  outputMinValue ← outputWaveValues[j];
                  outputMinIndex ← j;
      end
      j←j+1
      end
      end
```

Table 5 Pseudocode for Phase Calculation using which the phase difference between the input signal and the output response is calculated

4.8 User Interface

The user interface is comprised of a back-end data collection system that receives data from the Bluetooth and filters, stores, and analyzes the data. It collects all the data being sent at the COM port of the PC using Cable Replacement Algorithm and saves it into a text file. It is also responsible for sending all commands and test parameters to the dsPIC33F that is collected by the front-end. The front end is comprised of a Python-script web-based user interface that allows users to enter testing parameters for both the tests. The system is designed in such a way that the python backend can be running on a machine local to the device, and the graphical user interface can be running

on any other networked machine. The steps required to load the web interface on a local host are provided in Appendix 2. The initial screen displays the working title of the test along with some information about the tests and types of sensors to be attached and then the user is directed to go to the next page to fill out the test parameters using a button as shown in Figure 4-16 below.
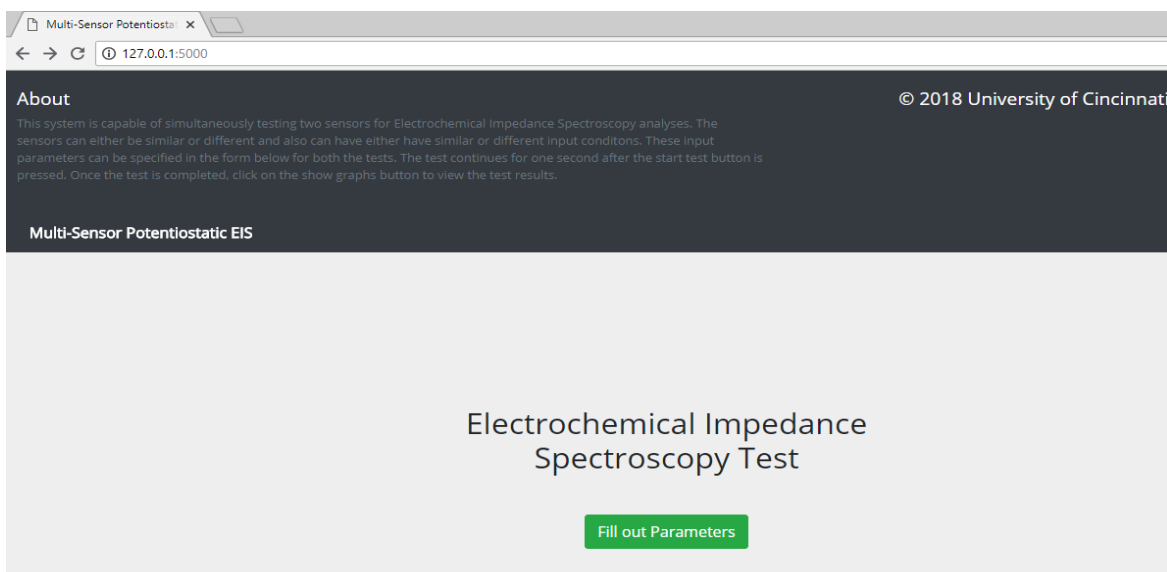

Figure 4-16 User Interface based on Flask WebApp

There are four main parameters to be filled by the user for both the tests namely, start and stop frequencies for the tests, the input amplitude and the amplifier gain as shown in Figure 4-17 on the next page. To run two similar tests, the user is advised to enter exactly similar or default configuration for the tests. To run two different EIS tests with change in frequency band and amplitude, the user can enter new values on this page. The test runs for about 60 seconds and at the end of the interval the show result button becomes active that processes the text file obtained from the test and presents the data in the form of a Bode plot.
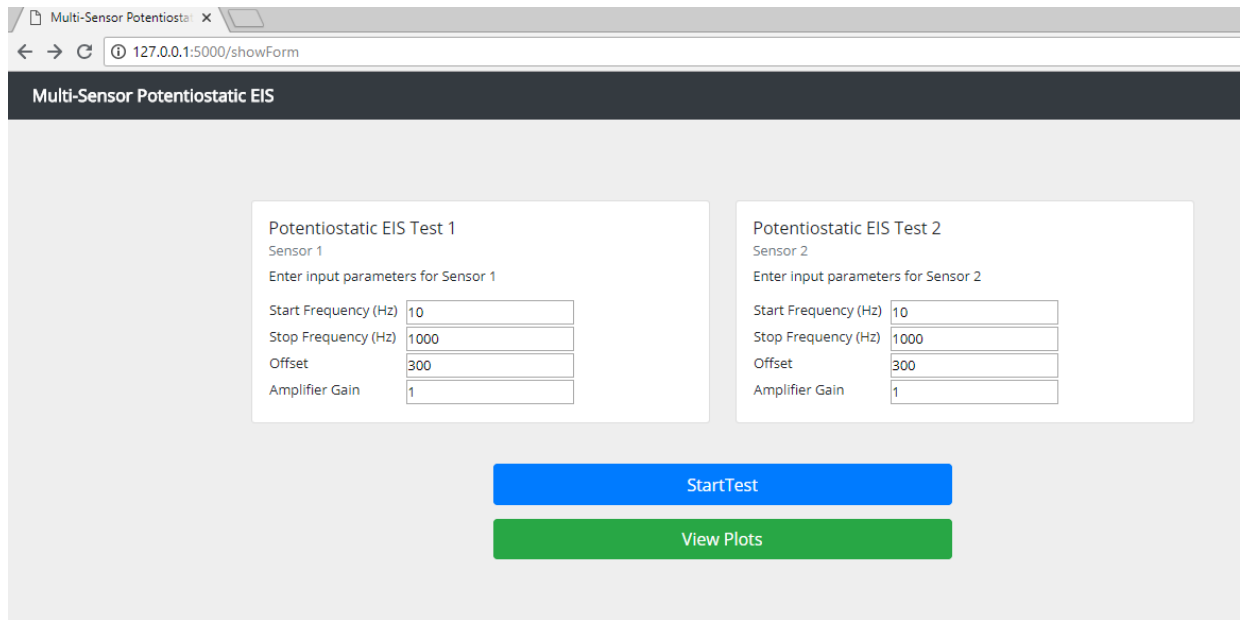
Figure 4-17 User interface input parameters form page

4.9 Printed Circuit Boards (PCBs)

Two designs have been created while prototyping and testing the system modules separately. The first run as shown in Figure 4-18 was specifically designed to test out each of the modules and configurations for stimulus signal generation and simultaneous ADC sampling. It was a wired connection making it easier to debug and enhance both the stimulus signals response from the ADCS.
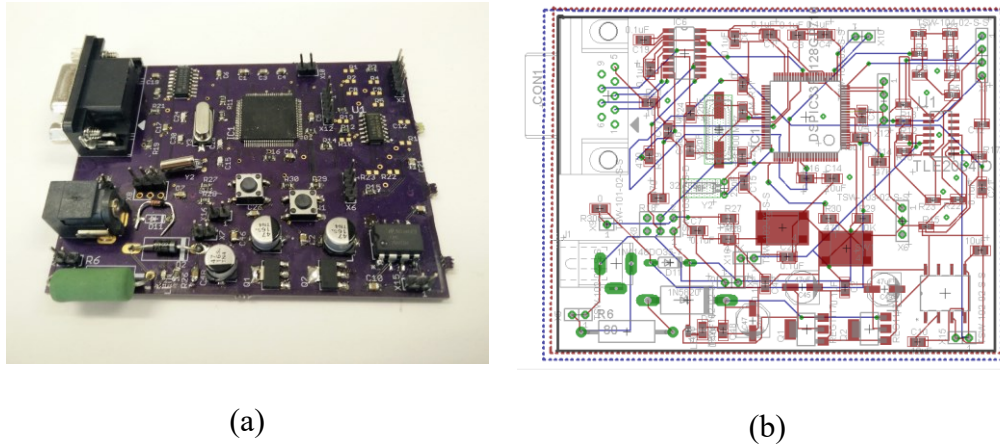
(a)   (b)

Figure 4-18 Printed Circuit Board of the first prototype

This design was extensively tested on with electrical circuit equivalents to yield good results. Once the stimulus signals and response collection were established, the second circuit was developed to interface and test out the analog circuit interface. Again, a total of two analog interface circuit designs were testes out with the first PCB and once the amplifiers were finalized, the second PCB design was finalized. It also featured the addition of BLE module for wireless connectivity, however this module was developed outside of the current PCB and can be interfaced to the main board easily. The power management board also had its iterations and finally a simple and stable design was chosen which provides power to both the main PCB and the BLE module. In the end Figure 4-19 shows a schematic circuit diagram for the board that has been designed for mounting all the peripherals including the filters, operational amplifiers and the dsPIC. More information on the schematic software, parts, integrated development environment and vendors that are used in for the hardware and software of this device is given in Appendix 3.
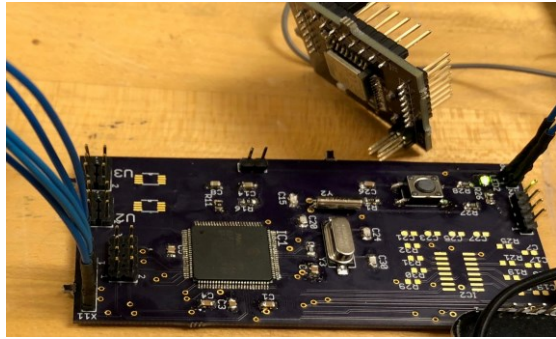
(a)
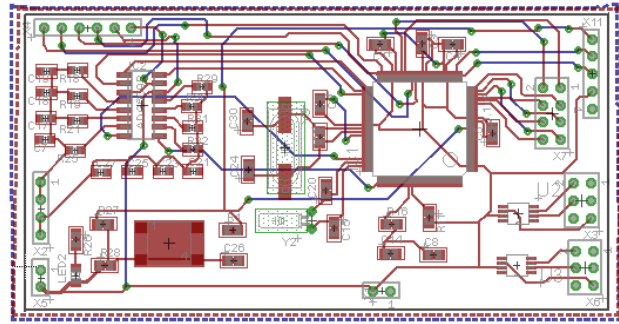
(b)

(c)
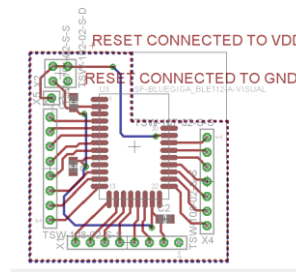
(d)

Figure 4-19 Printed Circuit Board of the second board design

The second design of the system which is a two-metal layer board layout was completed using EAGLE^{TM} board layout software. The board design showing all traces and connects to various electrical components is shown in Figure 4-20. It consists of the power management module, signal generation module, analog circuit interface and interconnects to sensors, programmer and Bluetooth module. The dimensions of the board are 86 mm * 87 mm.
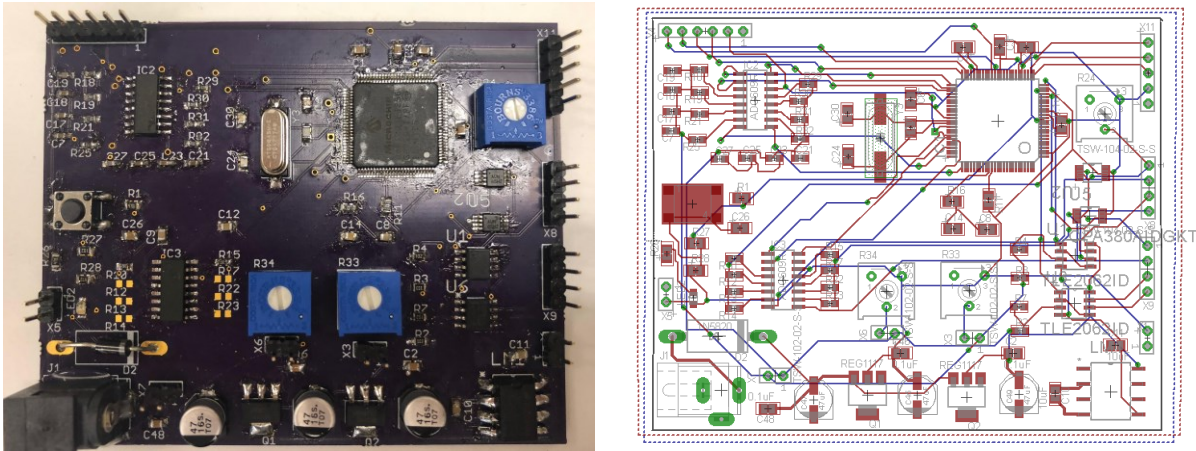
Figure 4-20 Printed Circuit Board of the final board design (1ˢᵗ prototype)

4.10 Integration and Working of System

As shown, the individual blocks are integrated to form a complete EIS system. The system is designed to work and adapt to both two electrodes and three electrodes electrochemical cells. The only hardware change between a two-electrode and three-electrode cell is the connection of the reference electrode to the counter electrode. The spectroscopy process is initiated with the calculation of the solution resistance (R_{sol}) of the cell. This is accomplished by passing a DC voltage across the cell and measuring the current across it. When using an equivalent circuit, the current is measured across the whole circuit.

The second step is then to measure the current across the cell by sending an analog sine wave stimulus over the specified range of frequency. This current is then converted to voltage by using a current to voltage converter (I-V). The output voltage is compared against the input voltage that is used as the reference. An algorithm in software calculates the magnitude of the impedance with respect to the reference by calculating the peak to peak voltage (V_{P-P}) of the output wave. The algorithm can calculate the peak-to-peak voltage over the frequency range and transfers the data via UART to a terminal. The second algorithm calculates the phase difference between the reference and the output wave. This is done by calculating the time difference between the zero crossings of the wave over an average of wave cycles. A timer is used to calculate the timer ticks of the zero crossings that are converted into time. The data is then transferred to a terminal for plotting the Nyquist and Bode plots.
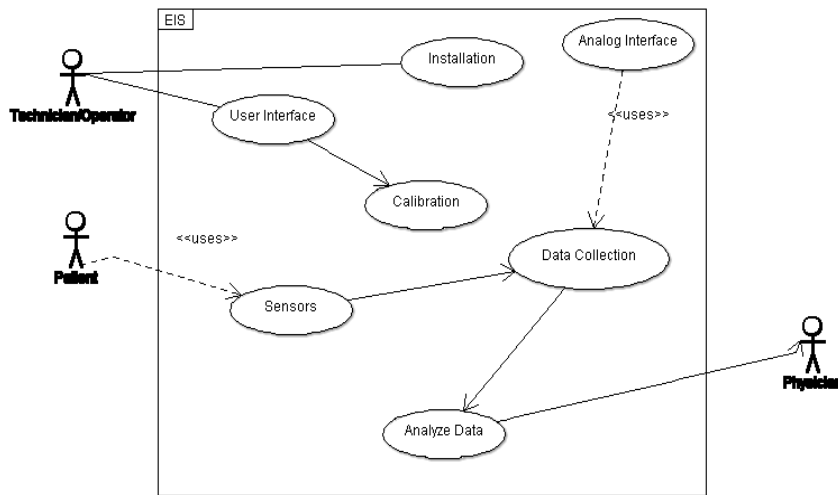
Figure 4-21 Use case diagram of the EIS system

A Use Case diagram of the system is shown in Figure 4-21. Since, the system is aimed to be used for health monitoring applications, a patient-physician setting is considered for understanding the system better. The system requires an operator who gets the system started and ready for use before the testing begins. A calibration function is included in the system design that enables calibration using a resistive circuit. Another important feature is the user interface that helps in collection of data samples into a file on the terminal. The flowchart for the entire test is shown in Figure 4-22.

Figure 4-22 Flowchart of the process flow

5. System Testing and Results

In this chapter, we present the results from systematic testing from each of the modules conducted as a part of the developmental process 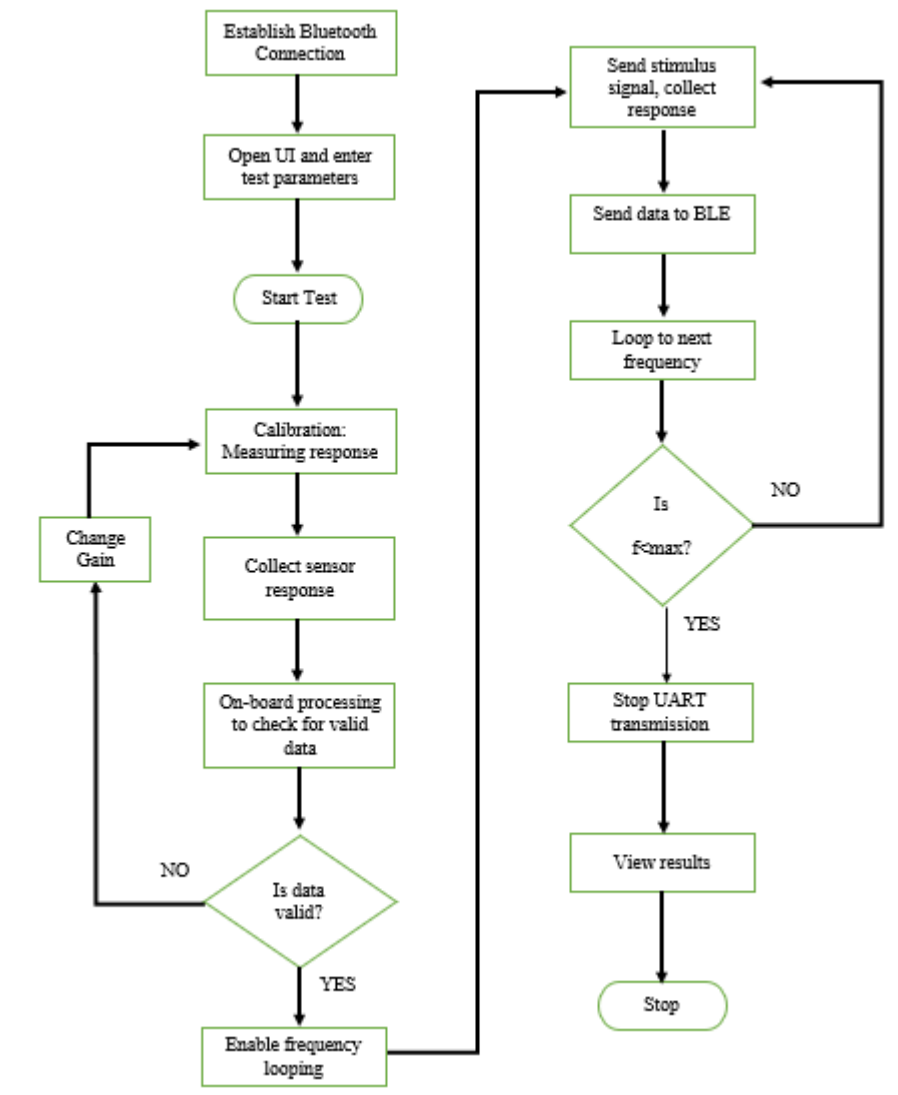of the entire system. This includes testing of input signal generation module, data acquisition module, wireless connectivity module and user interface. Next, we subject the system to different types of cells which include equivalent circuit analogs and electrochemical cells with varying impedance ranges. We also discuss issues, results, limitations, and lessons learned from both the developmental and final system testing experiments.

5.1 Preliminary Results

We first present results from developmental testing, including component-based testing of individual modules in the design.

The general test objectives were:

- To determine the correct signal generation of input sinusoidal waves for both the test cells.

- To identify correct simultaneous sampling of four input ADC channels with no phase difference visible.

- To identify correct data packet availability from the user interface to the microcontroller.

- To identify the number of sample losses during sensor information transmission through the wireless network.

5.1.1 Testing of Input Signal Generation Module

This test is done to determine if the signal that is being generated by the input signal generation module is at the required correct frequency. To test this, a sinusoidal wave at 200 Hz is generated and is applied to the dummy cell and the response signal is collected. From the graph in Figure 5-1, it is evident that the response signal is different in magnitude and phase which accomplishes the test. The amplitude of the signal applied here is 3.2 V. This is not the amplitude that will be applied to electrochemical cells but here it has been used for simplicity.
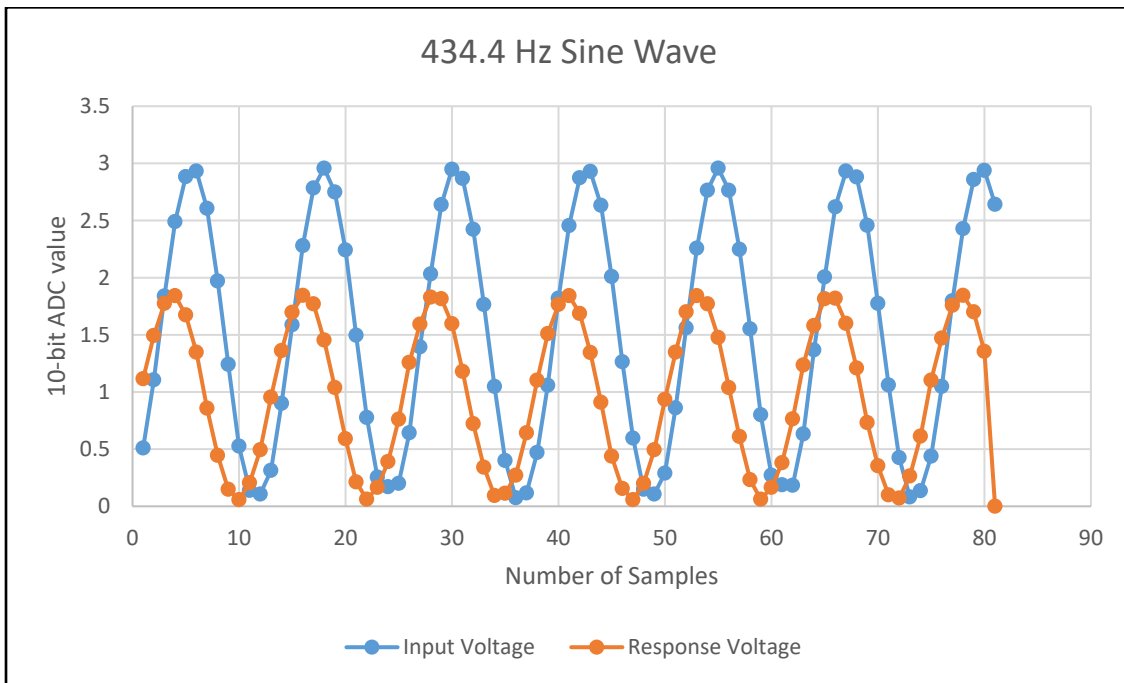
Figure 5-1 Input signal testing

5.1.2 Testing of Simultaneous Sampling of Data

For simultaneous testing of data sample four similar inputs are applied to four different ADC channels and then the data is collected and plotted. The four channels are CH0, CH1. CH2 and CH3 and the inputs are applied to analog input pins AN0, AN1, AN2, and AN3 respectively. The amplitude is again 3.2 V and the generated wave is at 200Hz.

Figure 5-2 Simultaneous sampling of fourADC channels tested at 200Hz

From the figure above, it can be seen that the four different sine waves collected from the ADC channels correctly sit on top of each other showing no phase difference or sampling anomalies as required. This shows all the four channels of the ADC enabled and set for simultaneous sampling of sensor data are functioning as expected.

5.1.3 Amplitude Attenuator Testing

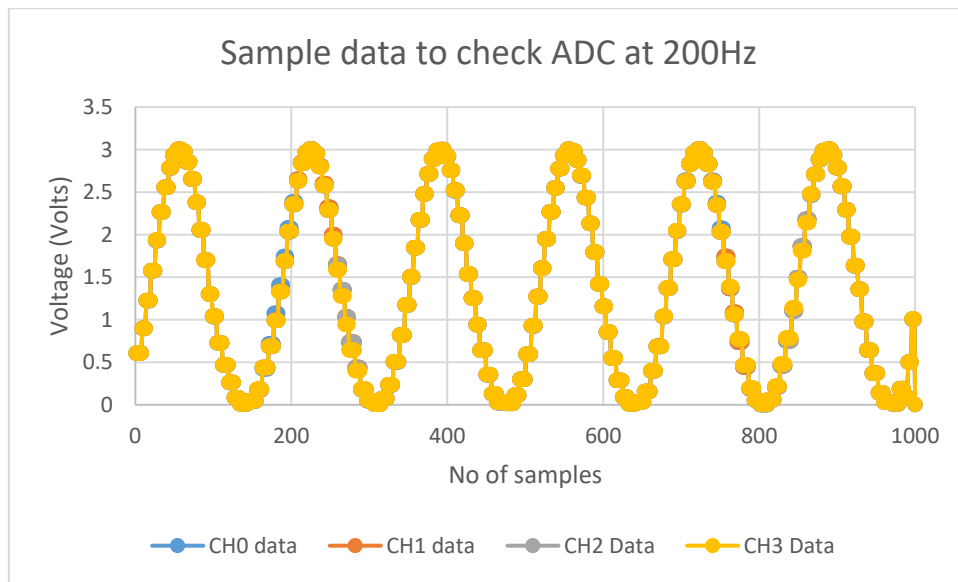This test is done to verify the voltage divider circuitry. The input signal to the voltage divider is plotted against the output signal. As can be seen there is significant attenuation in amplitude from 3.2 V to around 600 mV.
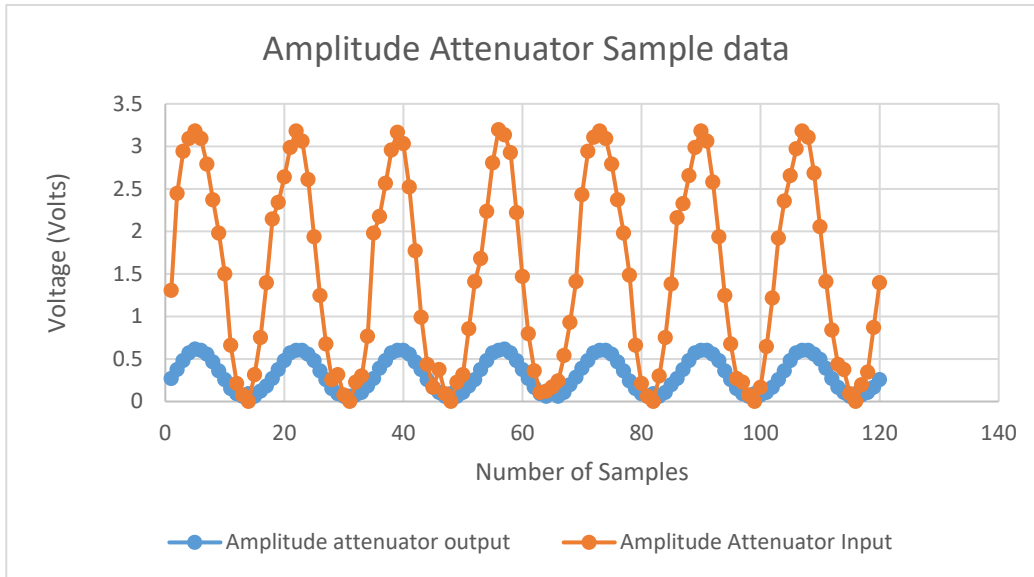
Figure 5-3 Amplitude attenuator testing shown with the help of a sample data

From the Figure 5-3 above, it can be observed that the output of the amplitude attenuator is significantly lesser than that of the input. This shows that the input attenuator circuit is correctly attenuating a 3.3V sinusoidal input wave to a 500mV output wave which is further reduced in amplitude using software for application as stimulus to electrochemical sensors.

5.2 Electrochemical cells testing

The device is validated by using the Universal Dummy Cell 4^{TM} [53]from Gamry Instruments, which includes a printed circuit board having two test cells equipped with terminals, arranged on the edges of the printed circuit board. One of the test cells is a Randle's cell, the circuit diagram of which is shown below in Figure 5-4.
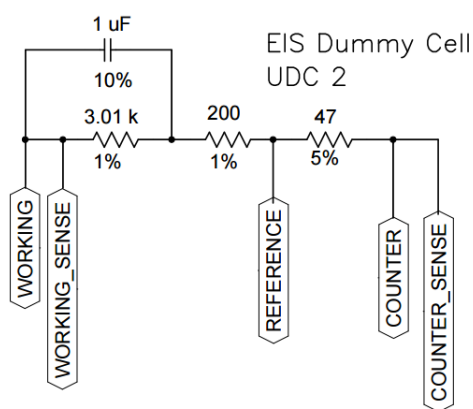
Figure 5-4 EIS Dummy Cell Schematic Diagram [53]

Finally, the device is tested on two electrochemical sensors one fabricated in lab consisting of a rod-based Ag/AgCl working electrode with Pt wire as Counter electrode. It is tested in 15 ml of milk solution at the same time a validation experiment is done on Gamry Instrument Reference 600. The second testing is for simultaneous measurements and the system is tested with two screen printed electrodes from DropSens which has an Au Counter and Working electrode and Ag Reference electrode.

5.2.1 Procedure

To test the electrochemical cells, the following procedure described is followed. This procedure ensures all the connections between the system and electrochemical cells are made before testing

beings. The user interface then sends the start command to the microcontroller which begins the test. The input signal generated as well as the response signal are then collected using the data acquisition system wirelessly. Then the magnitude and phase are calculated using a backend Python application and finally, the results are displayed.

The following checks are done before starting the test

- Ensure the counter, reference and working electrodes of both the cells are connected to their respective connections on the board.

- For two electrode cells, the counter and reference electrodes of both the cells must be tied together.

- Ensure the jumper pins of bias voltages to be provided to the electrochemical cell inputs are connected.

- Ensure the wireless connection is made

After the test is over, the following visual checks must be made before data processing is done

- Ensure the file name and time of the text file where the data is collected is correct

- Check for the starting and stop flags on the file to ensure complete data collection

- Check whether all the packet values are below the reference voltage limit of the ADC

5.2.2 Results

Calibration Circuit -Resistors Testing

The induvial systems have been tested with the calibration circuit on the Universal Dummy Cell 4 as shown in Figure 5-5. The calibration cell from Gamry is a 2 kΩ resistor connected between working electrode and counter electrode. For this experiment, it does matter if the cell is connected in a two-electrode or a three-electrode configuration as there are physical capacitances present between counter electrode and reference electrode. Because of this reason, we decided to run this test on two-electrode configuration there by connecting the counter and reference electrodes together and measuring the cell voltage between working and reference electrodes.
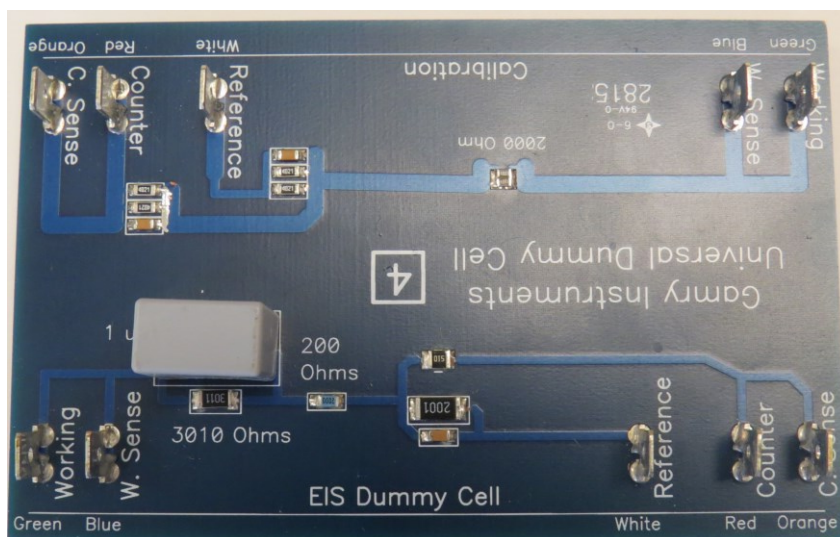
Figure 5-5 Picture of the Universal Dummy Cell 4 from Gamry Instruments that is used for calibration and initial system testing purposes [53]
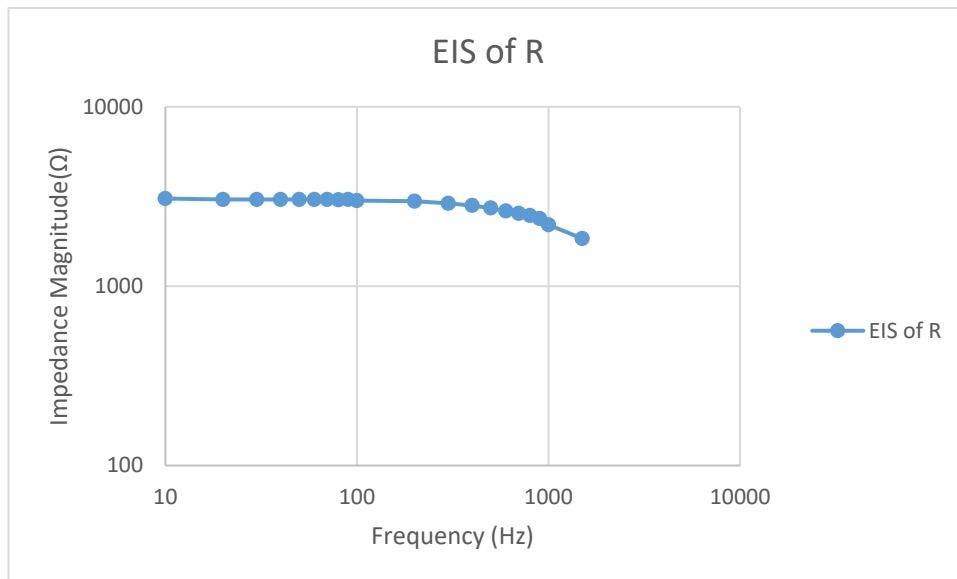
Figure 5-6 Experimental results using the EIS Dummy Cell 4 in calibration mode showing modulus of impedance for a resistive circuit

The results obtained from the device system are shown in Figure 5-6. We are expected to see a charge transfer resistance of 2 kΩ in the real part of impedance on the Bode Plot Since, we are measuring the total cell impedance we observe a total resistance which is slightly higher than the 2kΩ resistor that is connected between counter and reference electrode. However, the real impedance values are consistent throughout the frequency sweep indicating the presence of a resistive quantity between counter and working electrode. Since there is no capacitance present it this circuit, no phase change was observed all through the cell and phase calculations have been omitted for this test.

Universal Dummy Cell Results

The Universal Dummy Cell 4™ as shown in Figure 5-5 from Gamry Instruments is connected in a three-electrode configuration for this test. The cell is a RC circuit in parallel along with another resistance in series between the reference and working electrode. We are expected to see a phase change here between the voltage applied and the response collected due to the presence of a capacitive element. We test this again in a two-electrode configuration with the cell voltage being measured working and reference electrode and the reference and counter are tied together. The voltage applied for this test is 0.5 V and the current measured is in the range of microamps.

The Bode Plot showing the results of the magnitude and phase of impedance are shown in Figure 5-7. We can observe the change in impedance of the cell both in magnitude and phase as the frequency decreases from 1.5 kHz to 10Hz. The results are validated with testing the same circuit in a two-electrode configuration on the bench platform Reference 600 from Gamry Instruments. We observe a continuous rise in impedance as the frequency decreases which is an indicative of the increase in response current as the test proceeds. The device results do show an initial increase in response current as the frequency increases but towards the slower frequencies there is a decrease in impedance observed. This can be explained by two possibilities; one, the input magnitude for this test was a high on 500mV and due to the amplitude attenuation was not kept entirely constant. It changes throughout the test and therefore, we see a decrease in impedance towards the lower frequency band.
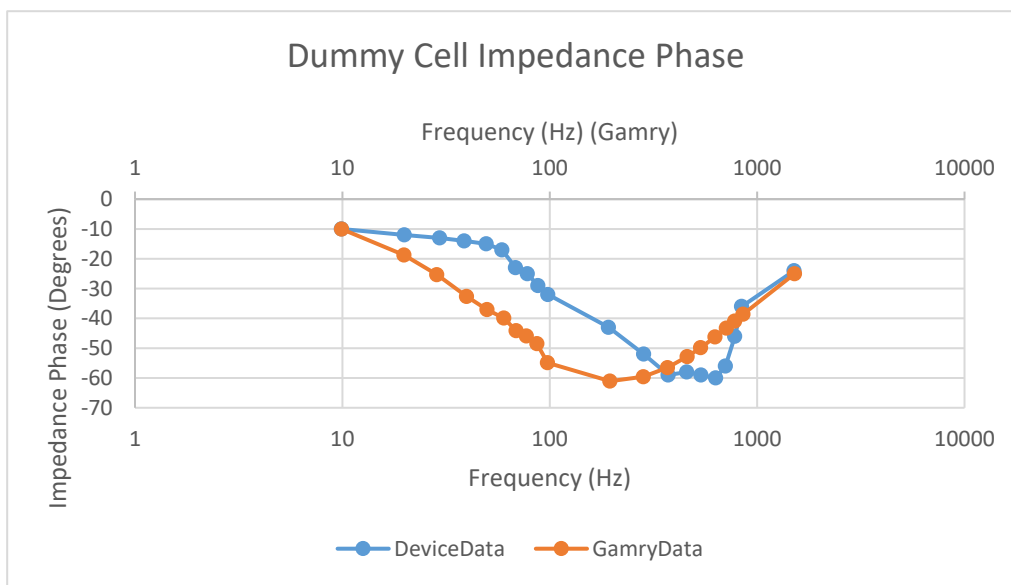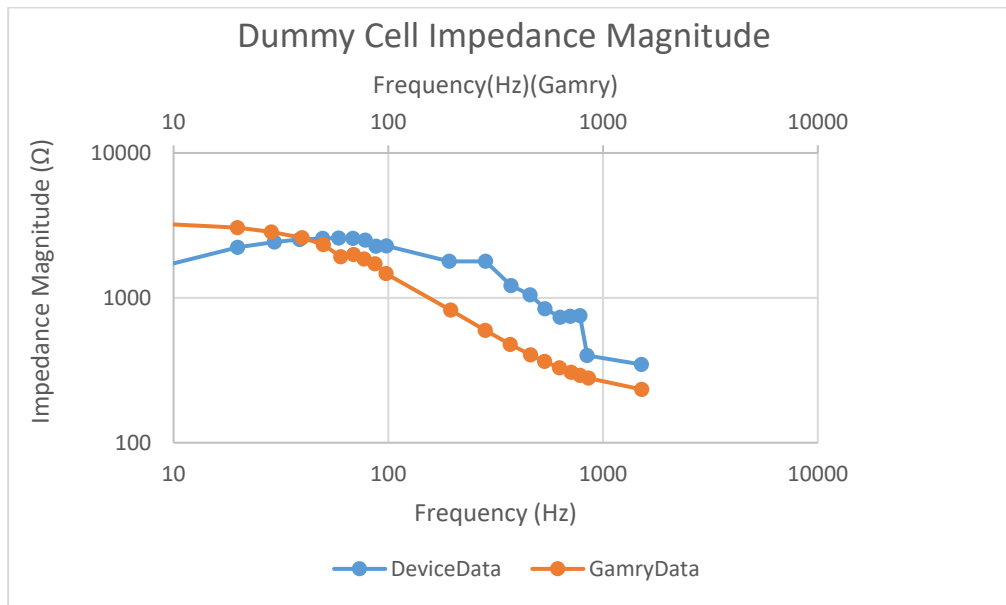
Figure 5-7 Experimental results using the EIS Dummy Cell 3 showing modulus and phase of impedance

Also, the phase change happens faster and towards the end of the frequency band, we observe a continuous series of values. This is attributed to the lower resolution of the algorithm being used to calculate the phase change between the voltage and current responses. This test proves to be very informative as it brings out the fallacies in the system. The choice of configuration systems such as two, three-electrodes plays an important role in the outcomes of the tests. For currents as high as in the range of mA, it is recommended to use a three-electrode configuration as it makes the system more stable and helps to maintain a constant potential between the reference and counter electrode.

Electrochemical Cell Results

The previous tests on equivalent circuit analogs prove to be educational in understanding the type of configurations that are to be used with electrochemical cells. We used a two-electrode configuration for a cell that returns a high current in the range of mA and observe a slight decrease in output response current as frequency seep happens. Therefore, for all the electrochemical cells we test from there on, we use the three-electrode configuration. Also, for electrochemical cells, the magnitude of voltage being applied to the cell is important as a very high voltage could trigger any unwanted chemical reactions thereby providing unusable results and damaging the cell. We still test one such electrochemical cell with different voltage ranges to prove this hypothesis and we observe that the best results are obtained at lower voltage levels. We perform tests on two different types of electrochemical cell types with different electrode areas and materials. All these cell tests are validated using the benchtop potentiostat Reference 600 from Gamry Instruments.

a. Cell 1

The first cell is a rod based electrochemical Ag/AgCl working electrode with 2mm diameter, Pt as Counter electrode and a Pt wire as Reference electrode. The electrochemical cell is tested with whole milk as solution and the results are also validated using Gamry Instruments Reference 600 Potentiostat [54] using the same input conditions. An input voltage of 100mV is applied to the counter electrode and the response current is collected into the ADC via the working electrode. The experimental setup for the following experiment is as shown in Figure 5-8 and the corresponding results of the test are shown in Figure 5-9.

Figure 5-8 Experimental setup for rod-based cell

From the results in Figure 5-9 we can observe the two curves from the device and Gamry are close to each other in magnitude. This attributes to the three-electrode configuration in which the cell has been connected now. In this configuration, efforts are made to maintain a constant voltage to the counter electrode. The use of control amplifier with three-electrode system helps in achieving the constant amplitude of voltage. The amplitude that has been provided to both the cells is 100mV. As it can be seen from the curves, there is a slight amplitude and phase variations between the data obtained from the Gamry potentiostat and the device potentiostat.

There are two reasons that could be causing the amplitude and phase variations between the two devices. Firstly, it accounts to the duration of the pulse being applied to the cells. The Gamry potentiostat applies the input voltage is small bursts of time before switching to the next frequency. The device we present applies the input voltage at a certain frequency for a total of 2 to 3 seconds before switching to the next frequency. This is limited due to the sampling speed of the analog-to-digital converter of the microcontroller in use. Continuous application of the input voltage at one frequency which lasts for 3 seconds can possibly alter certain electrochemical processes thereby producing an offset in the results as compared to that of the Gamry potentiostat. Secondly, the measurements obtained from the Gamry potentiostat start at 1MHz and sweep down to 5Hz while the measurements obtained from the device under test start at a lower frequency range of 1.5 kHz and sweep down to 10Hz. There is a possibility of many reactive processes being altered in the cell due to the absence of higher frequency ranges.
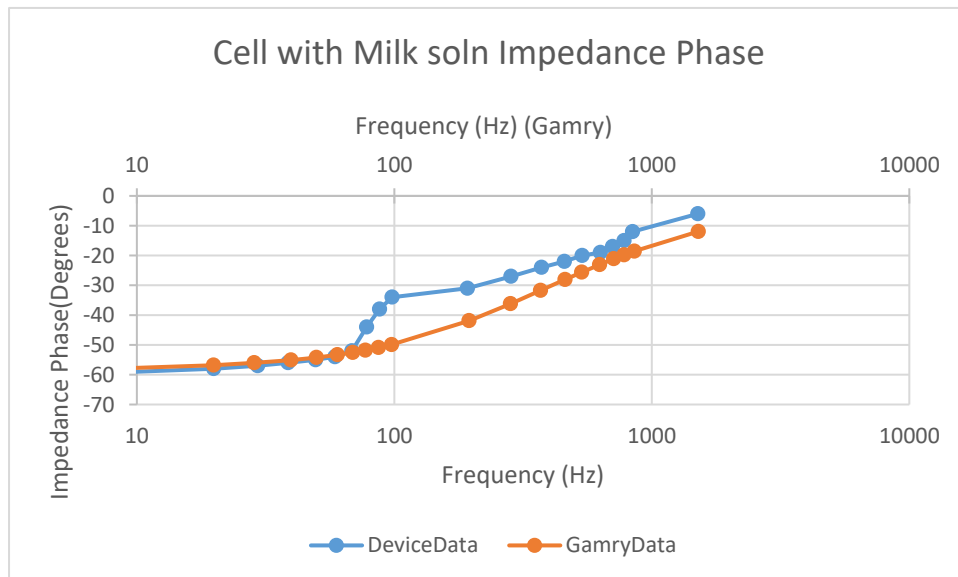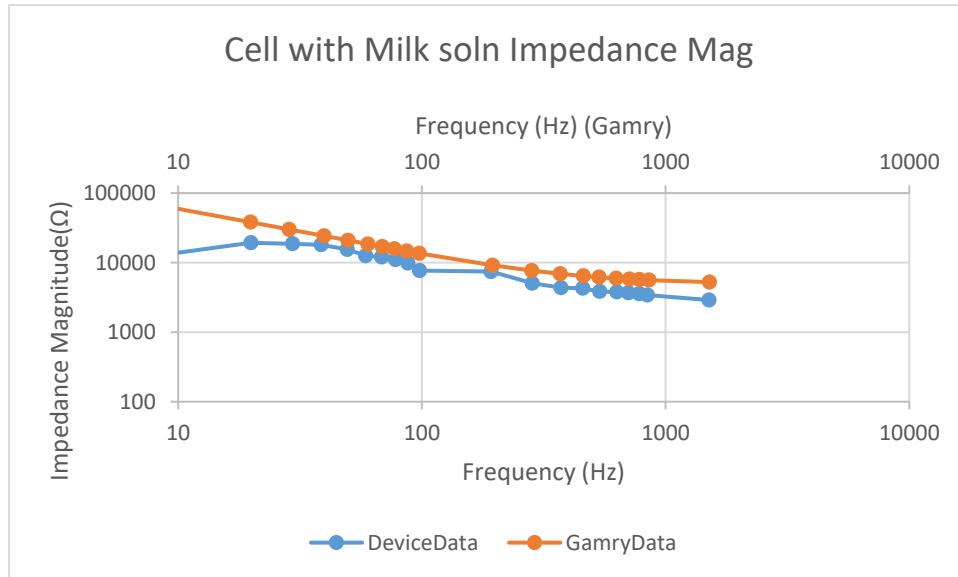
Figure 5-9 Experimental results using an electrochemical cell showing modulus and phase of impedance

b. Cell 2 and Cell 3

In this experiment, the electrochemical cell used is a screen-printed electrode called DropSens 550. The configuration for this cell is different from the one used before. It has a 4mm wide Au working electrode with Au counter and a Ag reference electrode. This cell can be tested in a liquid solution of as low as 50uL. A voltage of 100mV is also applied to this electrochemical cell and two solutions are tested with the three-electrode configuration. This similar setup if first tested with Gamry Reference 600 potentiostat for several tests runs in the interval of 20 minutes. After this, the same electrochemical cell is tested with our system for a total of three runs also at an interval of 20 minutes. Two electrochemical solutions are tested with this setup, one is 50ml of whole milk and second is 50 ml of PBS at a pH level of 7.4. The system is also tested using the IDE as shown in the Figure 4.3 and a buffer solution Phosphate-buffered saline (PBS) is used to cover the entire area of the IDE. PBS is a water-based salt solution containing sodium phosphate, sodium chloride and in some formulations potassium chloride and potassium phosphate. This solution is used because the osmolarity and ion concentrations of the solutions match those if the human body. The pH of the solution prepared is 7.4 and it is isotonic and non-toxic to most cells.

Since, the system is now tested on different cells, the system behaves differently from the other cell and the results for milk and PBS are shown in Figure 5-10 and Figure 5-11 respectively. In both these experiments the electrodes were kept continuously dipped in their respective solutions and the surfaces were not cleaned between test runs.
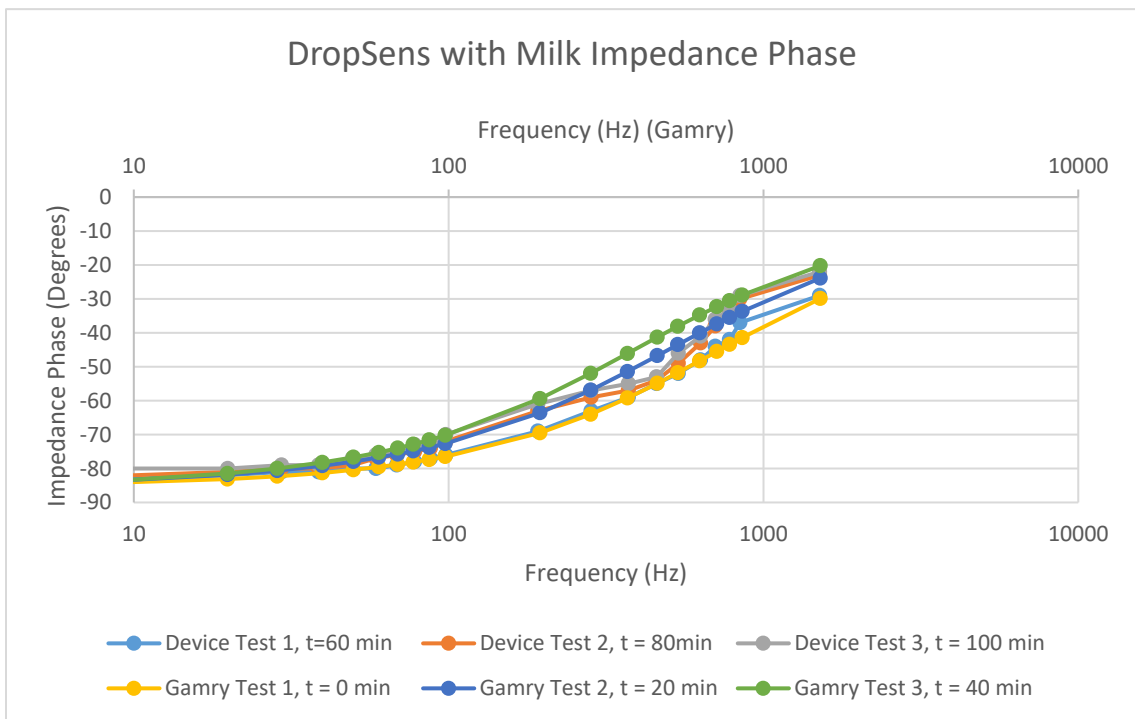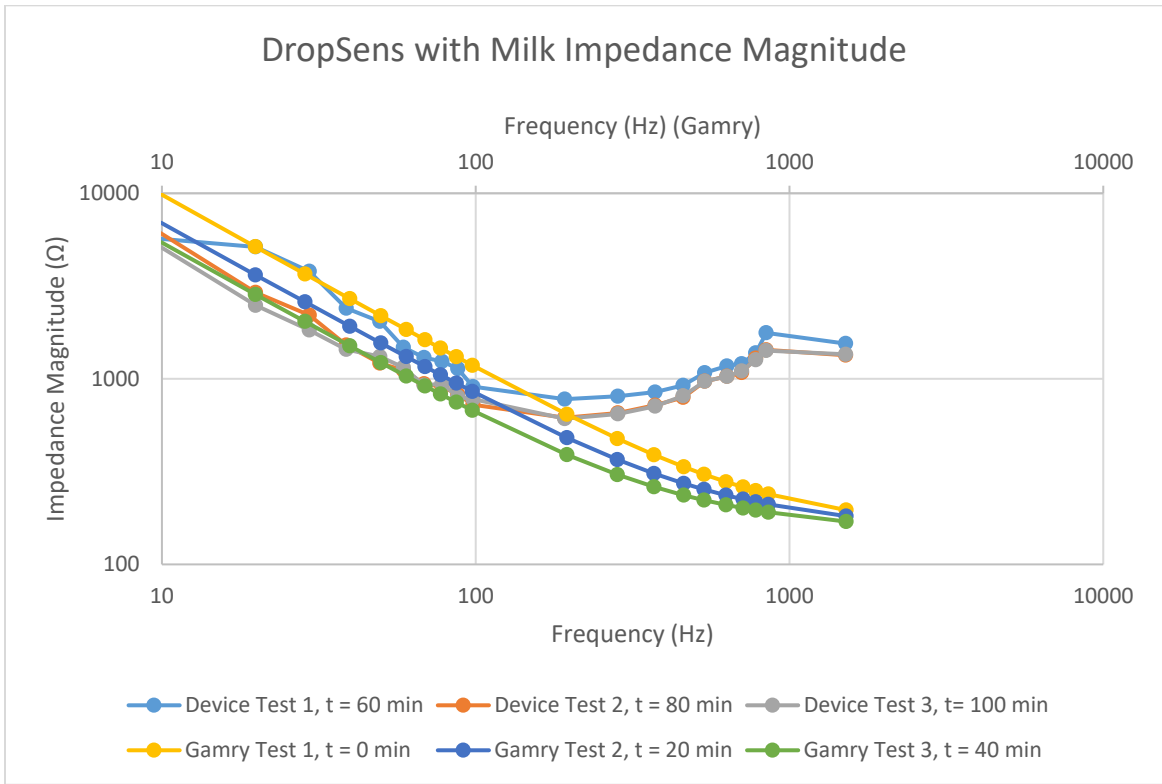
Figure 5-10 Experimental results using the DropSens electrode cells with whole milk as solution showing modulus and phase of impedance
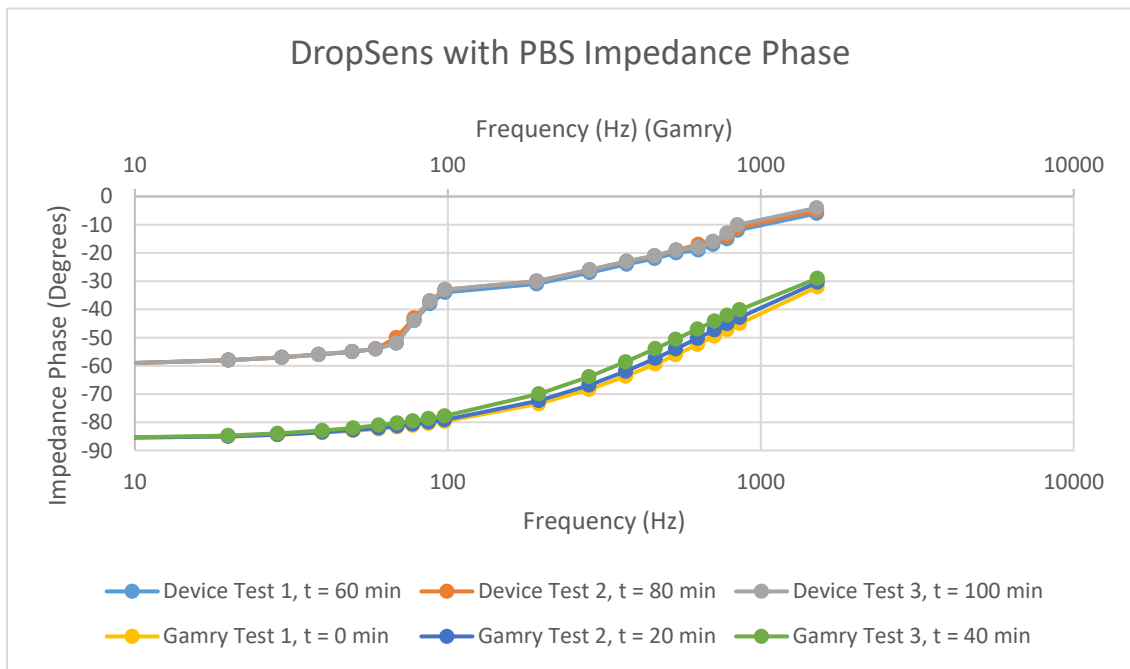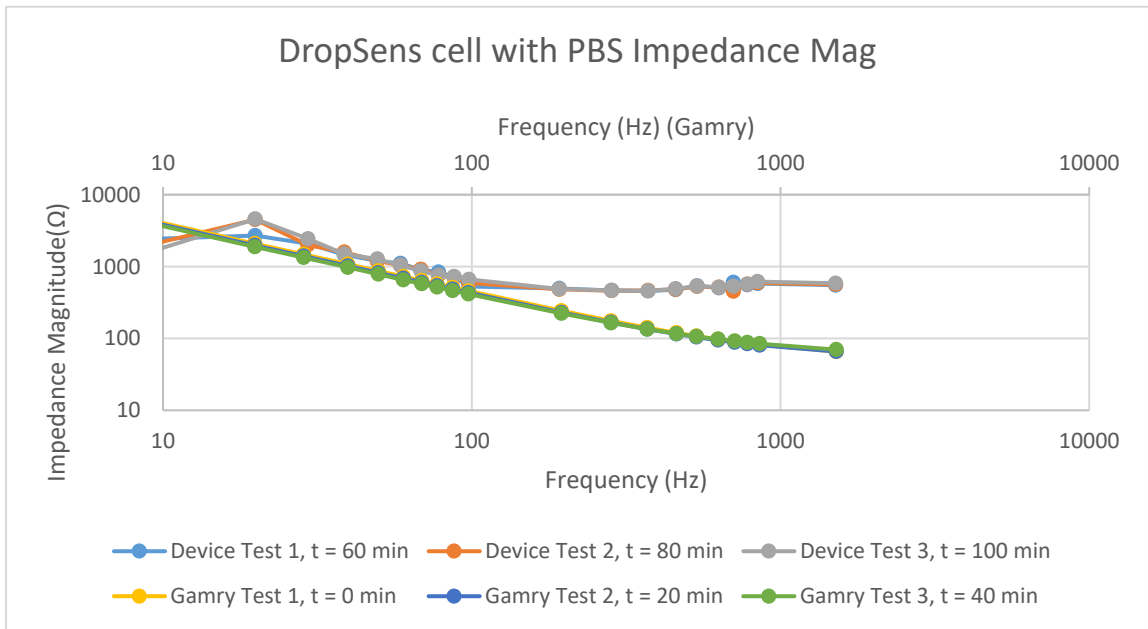
Figure 5-11 Experimental results using the DropSens electrode cells with PBS solution showing modulus and phase of impedance

From Figure 5-10, we can observe firstly the difference between the results obtained from the device and the results obtained from Gamry potentiostat. The initial increase in impedance and offset from the results obtained from device can be attributed to the systems inability to keep the voltage constant at high frequencies. This is again due to the 3db frequency amplitude attenuation of the filters used for sine wave generation. However, towards the mid spectrum, the input voltage does become constant and an expected trend is observed. We also observe that between each test run there is a decrease in impedance levels of milk and it continues to decrease as time increases whether the cells are tested on the Gamry potentiostat or the device. The reason for this behavior can be the result of the Au working electrode which is considered less stable than the Pt working electrode. Even the results from Gamry potentiostat are showing the same behavior as opposed to the results from the previous electrochemical cells tested with Pt working electrodes.

From Figure 5-11, we observe the results of the same tests being conducted with the similar cells and electrode setup, but on PBS solution. As we know, we can still observe the initial increase in impedance and offset from the results of our device as compared to Gamry potentiostat which is due to the stimulus voltage being slightly variable during that frequency band. We also observe that the results between tests do not change in the PBS solution and these are both validated by the Gamry potentiostat as well the device under test. W

    a. Two Screen Printed Electrode Cells tested on different solutions

In this experiment, the two cells, one with PBS and other with milk are tested simultaneously and the test is repeated twice. We can observe in both the runs that there is significant difference between the results of two different cells.

Figure 5-12 Experimental set up for simultaneous testing of two screen printed electrochemical cells

The two cells, Cell 1 with 50 ml PBS at pH of 7.4 and Cell 2 with 50 ml of Milk solution have been tested simultaneously. A voltage of 100 mV is applied to both the cells however the amplitude of the input stimulus can be changed between cells. The test is run from 1. 5 kHz to 10 Hz for both the cells and it is necessary to mention that this frequency range can also be changed to be different for both the cells in test.

Figure 5-13 Experimental results using the DropSens Electrode cells for simultaneous EIS measurements showing the magnitude and phase of cell impedance for different solutions

The results of the simultaneous measurements are shown in Figure 5 -13. From initial observance of the data, it is easy to identify the presence of different impedance ranges and their repetitions indicating that the device is measuring two different response currents simultaneously. The second observance is to identify a possible difference between the PBS and Milk results. Since, we have already tested these similar cells one after the other in our previous test, where we observed the change in impedance amplitude for the milk solution while the impedance amplitude for the PBS solution remains the same. This similar behavior can be observed in the simultaneous testing of both the cells indicating yet again that the system can identify two different current responses from two different electrochemical cells simultaneously. The input conditions and input stimulus generators for both the cells are different even though the same amplitude of 100mV is being applied to the cells. It is also important to note that the entire circuitry of one cell starting from the signal generation to the data acquisition is isolated from the another to avoid interference and unwanted noise.

b. Two Screen Printed Electrode Cells tested on same solution:

In this experiment, two cells, Cell 1 and Cell 2 with 50ml of PBS at pH of 7.4 are tested with PBS simultaneously and the test is repeated thrice. With each repetition, the PBS solution of Cell2 is diluted to 50% PBS by adding deionized water. A voltage of 100 mV is applied to both the cells however the amplitude of the input stimulus can be changed between cells. The test is run from 1. 5 kHz to 10 Hz for both the cells and it is necessary to mention that this frequency range can also be changed to be different for both the cells in test.
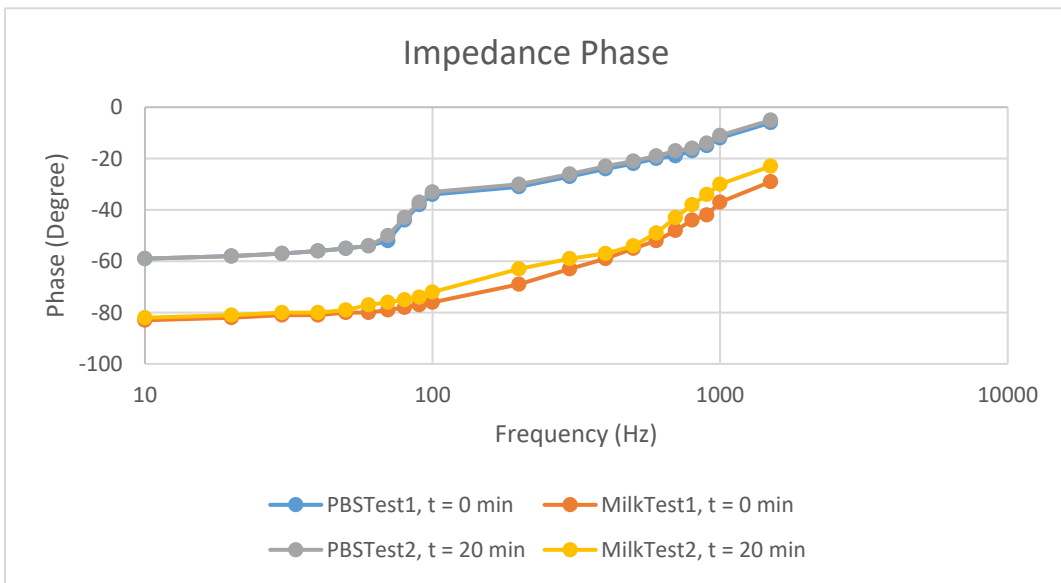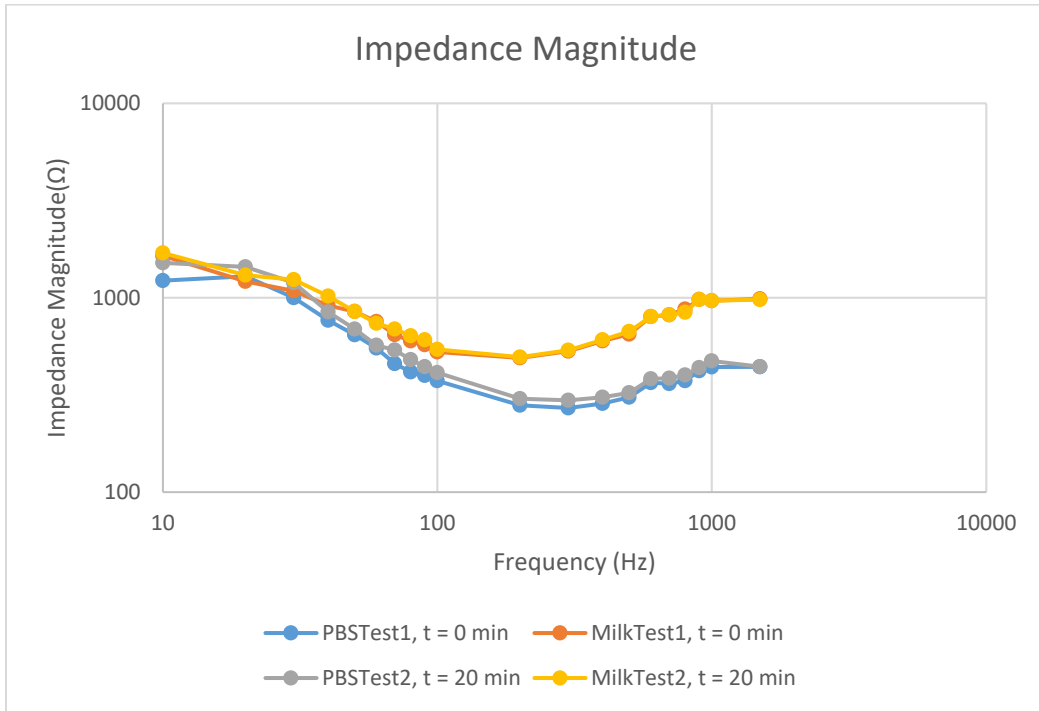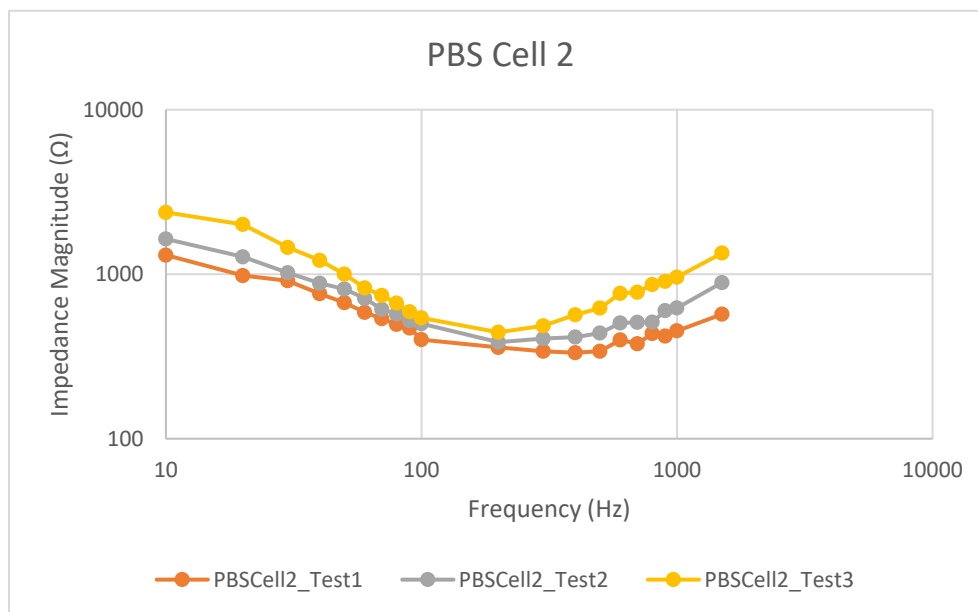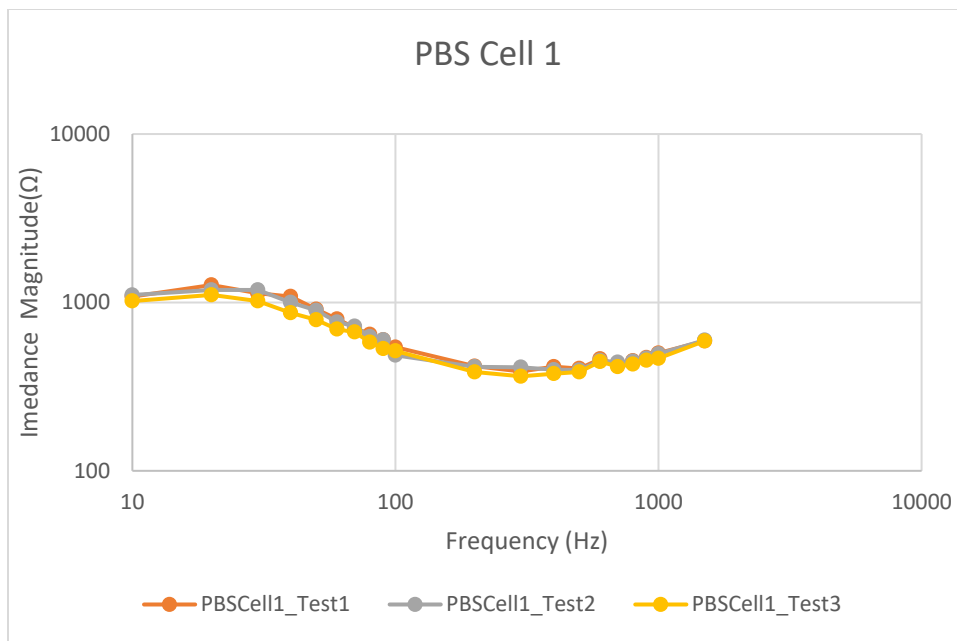
Figure 5-14 Experimental results using the DropSens Electrode cells for simultaneous EIS measurements showing the magnitude and phase of cell impedance for same solutions

The results of the simultaneous measurements with same solutions are shown in Figure 5 -14. From initial observance of the data, it is easy to identify the presence of different impedance ranges and their repetitions indicating that the device is measuring two different response currents simultaneously. The second observance is to identify a possible difference between the Cell 1 PBS and Cell 2 PBS results. Since the solution in Cell 2 is diluted after every test, a change in impedance is observed in Cell 2 with each repeated test while the impedance in Cell 1 remains same for all the tests. The input conditions and input stimulus generators for both the cells are different but the same amplitude of 100mV is applied to the cells. It is also important to note that the entire circuitry of one cell starting from the signal generation to the data acquisition is isolated from the another to avoid interference and unwanted noise.

Even with similar conditions and input stimulus applied to both the cells, the impedance difference when the buffer is diluted is recognized by the device. This is because a lesser amount of current is measured from the working electrode due to dilution of buffer solution by deionized water. This shows that the device can successfully measure different concentrations of biofluids simultaneously for two cells.

6. Conclusion and Future Work

Wearable biosensors are striving fast towards being ubiquitous closely monitoring human activities by analyzing biofluids without limiting motion. For these biomarker detections, many electroanalytical techniques have been used like cyclic voltammetry, square wave voltammetry. If bioimpedance analysis is performed on a spectrum of frequency, it reveals the frequency response of the system and is helpful for both diagnosis and characterization. Decentralization of diagnostic testing from large and expensive clinical laboratories directly to the patients' bedside or home has been a focus of researchers for many years and is a key component of the current precision medicine initiative. The objective of this proposal is to advance the contemporary portable EIS sweat biomarker analysis platform research for a sophisticated multi-sensor and multi-sine portable wireless platform. The device is aimed to be able to calculate the magnitude and phase of the impedance response collected from the electrochemical cell. Along with this, the device includes an analog interface circuitry with potentiostat for interfacing the device with electrochemical cells and filters for signal conditioning for the stimulus and responses procured by the electrochemical cell.

6.1 Summary

This section summarizes the research work presented in the thesis on development of a micro-controller based Electrochemical Impedance Spectroscopy platform for wearable health monitoring devices. The research considers two different approaches of performing EIS and puts forward solutions to develop a small form factor based EIS device. The first approach is to use the classical way of performing an EIS on an electrochemical cell which is by applying a small

amplitude sinusoidal signal sweep generated by the dsPIC and tracking the current response from the working electrode using an analog interface circuitry; the processing of which yields the characteristics of the electrochemical cell. The second approach is to use a different and easily producible square wave in place of sine waves and compare the results with respect to the classical EIS method.

In Chapter 2, the previous work on small form factor based EIS devices is discussed and the technique of EIS is explained in brief. Different approaches tried by various researchers over the period of last twenty years is brought under light and existing issues and challenges related to the development of portable EIS devices in the above scenarios are explained. Chapter 4 puts forward an EIS development system based on the dsPIC33F. It explains the salient features of the proposed system design such as signal generation using the PWM and filter thereby reducing hardware and cost, analog interface to the electrochemical cell and the signal processing module. In order to reduce the size of the system, signal generation is done using the PWM module available on the dsPIC chip and a low pass filter. Software in the IDE allows sweep of the frequency and at each frequency the magnitude and phase is calculated in the software additionally.

Chapter 5 presents the results obtained from the application of the developed EIS system design described in Chapter 4. The results signify the reliability and efficiently of the proposed system design as it is successful in determining the characteristics of the electrochemical cell with the requirements laid down in Chapter 3.

6.2 Conclusions

Wearable biosensors are striving fast towards being ubiquitous closely monitoring human activities by analyzing biofluids without limiting motion. For detection of these biomarker, many electroanalytical techniques have been used including cyclic voltammetry and square wave voltammetry. If bio impedance analysis is performed over a spectrum of frequency, the analysis reveals the frequency response of the system and is helpful for both diagnosis and characterization. Decentralization of diagnostic testing from large and expensive clinical laboratories directly to the patients' bedside or home has been a focus of researchers for many years and is a key component of the current precision medicine initiative. The objective of this research is to advance the contemporary portable EIS sweat biomarker analysis platform research for a sophisticated multi-sensor and multi-sine portable wireless platform. The device can calculate the magnitude and phase of the impedance responses collected from two electrochemical cells simultaneously. Along with this, the device includes an analog interface circuitry with potentiostat for interfacing the device with electrochemical cells and filters for signal conditioning for the stimulus and responses procured by the electrochemical cell.

6.3 Limitations and Future Discussions

From the literature review of EIS and its process, it is evident that the technique is popular and powerful and efficient in predicting the behavior of electrolytes in electrochemical cells. In addition to its popularity, it has a wide range of applications from corrosion behavior to health monitoring. This system has been developed to be able to serve as an on-chip EIS device and has been designed keeping in mind the requirements and constraints. Of the many requirements, the main objective is to be able to reduce the size of the system yet make it reliable and efficient. It is

already noted that the device can generate sinusoidal inputs on the chip and change the frequencies to produce the sweep. The device is also able to calculate the magnitude of the impedance correctly with less than 5% error both when the inputs are given as individual and in sweep. The system can detect phase changes between the input signal and output response and transmit it to a terminal wirelessly. However, there are several limitations to this device some of which are mentioned here and a direction to overcome them is also discussed.

1. The frequency range of the device is limited from 1 Hz to 2.5 KHz. This is because the PWM module can generate a PWM signal of only certain frequency and the number of samples in the sine wave greatly affect its frequency. This frequency can be significantly increased by lowering the number of samples of the sine wave. However, there is a requirement of larger number of samples as we are calculating the phase difference between each sample. There is a trade-off with each choice that we make, and the best possible option can be chosen according to the application or the frequency range one is interested to calculate EIS in. This limitation can also be overcome by using a different microcontroller with a faster speed that can generate faster PWM signals.

2. This system has been specifically designed as a proof of concept for two sensor testing. Also, many microcontroller features do not enable us to generate more than two different input signals and sample not more than 8 different ADC channels simultaneously. These limitations can be easily overcome with the use of different microcontroller.

3. The system consists of a web-based user interface that is connected via Bluetooth Low Energy and can read and save all the data in a text file and display the results. This application for now is limited to being used on a laptop. This similar application can be extended to be used on a phone with the help of a programming interface. However, the web-based application can be used either on the laptop or on the phone making it versatile.

4. This system can now differentiate between two different electrochemical cells attached to it however, extensive and exhaustive testing of the system is required to enable multi-analyte biomarker detection with different sample concentrations and sample sizes.

References

[1] J. Heikenfeld, "Non-invasive Analyte Access and Sensing through Eccrine Sweat: Challenges and Outlook circa 2016," *Electroanalysis*, vol. 28, no. 6, pp. 1242–1249, Jun. 2016.

[2] C. Tronstad, H. Kalvøy, S. Grimnes, and Ø. G. Martinsen, "Improved estimation of sweating based on electrical properties of skin," *Ann. Biomed. Eng.*, vol. 41, no. 5, pp. 1074–1083, 2013.

[3] M. J. Buono, C. S. White, and K. P. Connolly, "Cholinergic sensitivity of the eccrine sweat gland in trained and untrained men.," *J. Dermatol. Sci.*, vol. 4, pp. 33–37, 1992.

[4] O. Article, "Development of Multi-frequency Electrical Impedance Spectroscopy (EIS) System for Early Detection of Breast Cancer," pp. 26–33, 2013.

[5] B. Pejcic and R. De Marco, "Impedance spectroscopy: Over 35 years of electrochemical sensor optimization," *Electrochim. Acta*, vol. 51, pp. 6217–6229, 2006.

[6] C. Breitkopf, "Impedance Spectroscopy Old Technique – New Applications," 2012.

[7] V. Vijay, B. Raziyeh, S. Amir, D. Jelena, B. J. Alicia, B. Axel, M. Jan, C. Yihui, and H. Andreas, "High-density CMOS microelectrode array system for impedance spectroscopy and imaging of biological cells," *2016 IEEE SENSORS*. pp. 1–3, 2016.

[8] E. Juanola-Feliu, P. L. Miribel-Català, C. P. Avilés, J. Colomer-Farrarons, M. González-Piñero, and J. Samitier, *Design of a customized multipurpose nano-enabled implantable system for in-vivo theranostics*, vol. 14, no. 10. 2014.

[9] "Samiksha Nayak, Nicole R. Blumenfeld, Tassaneewan Laksanasopin, and Samuel K. Sia, Point-of-Care Diagnostics: Recent Developments in a Connected Age Analytical Chemistry 2017 89 (1), 102-123 DOI: 10.1021/acs.analchem.6b04630."

[10] A. Bogomolova, E. Komarova, K. Reber, T. Gerasimov, O. Yavuz, S. Bhatt, and M. Aldissi, "Challenges of Electrochemical Impedance Spectroscopy in Protein Biosensing," *Anal. Chem.*, vol. 81, no. 10, pp. 3944–3949, May 2009.

[11] Y. Chao, D. Rairigh, and A. Mason, "On-chip electrochemical impedance spectroscopy for biosensor arrays," *Proc. IEEE Sensors*, pp. 93–96, 2006.

[12] E. Angelini, A. Carullo, S. Corbellini, F. Ferraris, V. Gallone, S. Grassini, M. Parvis, and A. Vallan, "Handheld-impedance-measurement system with seven-decade capability and potentiostatic function," *IEEE Trans. Instrum. Meas.*, vol. 55, no. 2, pp. 436–441, 2006.

[13] "P. Bhatnagar and F. R. Beyette, 'Electrochemical impedance spectroscopy circuitry for biosensor applications,' 2017 IEEE 60th International Midwest Symposium on Circuits and Systems (MWSCAS), Boston, MA, 2017, pp. 1469-1472. doi: 10.1109/MWSCAS.2017.80532."

[14] P. Bhatnagar and F. Beyette, "Microcontroller-based Electrochemical Impedance Spectroscopy for wearable health monitoring systems," *2015 IEEE 58th International Midwest Symposium on Circuits and Systems (MWSCAS)*. pp. 1–4, 2015.

[15] F. R. B. J. Purva Bhatnagar, "No Title," in *Electrochemical Impedance Spectroscopy Circuitry for Biosensor Applications*, 2017, p. 4.

[16] B. H. Shadfan, A. R. Simmons, G. W. Simmons, A. Ho, J. Wong, K. H. Lu, R. C. Bast, and J. T. McDevitt, "A multiplexable, microfluidic platform for the rapid quantitation of a biomarker panel for early ovarian cancer detection at the point-of-care," *Cancer Prev. Res.*, vol. 8, no. 1, pp. 37–48, 2015.

[17] F. Villa, A. Magnani, M. Maggioni, A. Stahn, S. Rampichini, G. Merati, and P. Castiglioni, "Wearable Multi-Frequency and Multi-Segment Bioelectrical Impedance Spectroscopy for Unobtrusively Tracking Body Fluid Shifts during Physical Activity in Real-Field Applications: A Preliminary Study," *Sensors*, vol. 16, no. 5, p. 673, May 2016.

[18] A. Sun, A. G. Venkatesh, and D. A. Hall, "A Multi-Technique Reconfigurable Electrochemical Biosensor: Enabling Personal Health Monitoring in Mobile Devices," *IEEE Transactions on Biomedical Circuits and Systems*, vol. 10, no. 5. pp. 945–954, 2016.

[19] S. K. Vashist, O. Mudanyali, E. M. Schneider, R. Zengerle, and A. Ozcan, "Cellphone-based devices for bioanalytical sciences Multiplex Platforms in Diagnostics and Bioanalytics," *Anal. Bioanal. Chem.*, vol. 406, no. 14, pp. 3263–3277, 2014.

[20] Y. Hong, Y. Wang, W. L. Goh, Y. Gao, and L. Yao, "Analysis of monolithic I/Q based impedance measurement circuits: Impact of non-ideal circuit effects on accuracies," *2016 International Symposium on Integrated Circuits (ISIC)*. pp. 1–4, 2016.

[21] S. Grassini, S. Corbellini, E. Angelini, F. Ferraris, and M. Parvis, "Low-Cost Impedance Spectroscopy System Based on a Logarithmic Amplifier," *IEEE Transactions on Instrumentation and Measurement*, vol. 64, no. 5. pp. 1110–1117, 2015.

[22] A. A. Thulasi, D. Bhatia, P. T. Balsara, and S. Prasad, "Portable impedance measurement device for sweat based glucose detection," *2017 IEEE 14th International Conference on Wearable and Implantable Body Sensor Networks (BSN)*. pp. 63–66, 2017.

[23] D. P. Rose, M. E. Ratterman, D. K. Griffin, L. Hou, N. Kelley-Loughnane, R. R. Naik, J. A. Hagen, I. Papautsky, and J. C. Heikenfeld, "Adhesive RFID Sensor Patch for Monitoring of Sweat Electrolytes," *IEEE Transactions on Biomedical Engineering*, vol. 62, no. 6. pp. 1457–1465, 2015.

[24] C. I. Values, P. Electrochemistry, C. Elements, C. Equivalent, and C. Models, "Basics of Electrochemical Impedance Spectroscopy," no. 1.

[25] Autolab, "Electrochemical Impedance Spectroscopy (EIS) Part 6 – Measuring raw signals in EIS," *Spectroscopy*, pp. 1–3, 2011.

[26] D. Macdonald D.Digby, "Electrochemical Impedance Spectroscopy," pp. 2000–2008, 1992.

[27] B. T. Mark E Orazem, *Electrochemical impedance spectroscopy*. John Wiley and Sons, 2008.

[28] B. Le Gorrec and C. Montella, "Handbook of Electrochemical Impedance Spectroscopy," 2009.

[29] D. a. Harrington and P. Van Den Driessche, "Mechanism and equivalent circuits in electrochemical impedance spectroscopy," *Electrochim. Acta*, vol. 56, no. 23, pp. 8005–8013, 2011.

[30] G. a. Ragoisha and a. S. Bondarenko, "Potentiodynamic electrochemical impedance spectroscopy," *Electrochim. Acta*, vol. 50, no. November 2004, pp. 1553–1563, 2005.

[31] A. Application and N. Eis, "Electrochemical Impedance Spectroscopy (EIS) Part 4 – Equivalent Circuit Models," *Spectroscopy*, pp. 4–6.

[32] P. Arpaia, F. Clemente, and A. Zanesco, "Low-invasive diagnosis of metallic prosthesis osseointegration by electrical impedance spectroscopy," *IEEE Trans. Instrum. Meas.*, vol. 56, no. 3, pp. 784–789, 2007.

[33] G. Instruments, "Reference 3000. Potentiostat / Galvanostat / ZRA Operator â€™ s Manual," *ReVision*, 2010.

[34] "Metroohm Autolab PGSTAT302N Operators Manual," 2017.

[35]   PalmSens, "Compact Electrochemical Interfaces Potentiostat / Galvanostat / Impedance Analyzer," p. 7, 2016.

[36]   J. Ferreira, F. Seoane, A. Ansede, and R. Bragos, "AD5933-based spectrometer for electrical bioimpedance applications," *J. Phys. Conf. Ser.*, vol. 224, p. 12011, Apr. 2010.

[37]   C. Margo, J. Katrib, M. Nadi, and A. Rouane, "A four-electrode low frequency impedance spectroscopy measurement system using the AD5933 measurement chip," *Physiol. Meas.*, vol. 34, no. 4, pp. 391–405, Apr. 2013.

[38]   U. Pliquett and A. Barthel, "Interfacing the AD5933 for bio-impedance measurements with front ends providing galvanostatic or potentiostatic excitation," *J. Phys. Conf. Ser.*, vol. 407, p. 12019, Dec. 2012.

[39]   S. Corbellini and A. Vallan, "Arduino-based portable system for bioelectrical impedance measurement," *2014 IEEE International Symposium on Medical Measurements and Applications (MeMeA)*. pp. 1–5, 2014.

[40]   N. Talukder, A. Furniturewalla, T. Le, M. Chan, S. Hirday, X. Cao, P. Xie, Z. Lin, A. Gholizadeh, S. Orbine, and M. Javanmard, "A portable battery powered microfluidic impedance cytometer with smartphone readout: towards personal health monitoring," *Biomed. Microdevices*, vol. 19, no. 2, p. 36, 2017.

[41]   T. A. Chen, W. J. Wu, C. L. Wei, R. B. Darling, and B. D. Liu, "Novel 10-Bit Impedance-to-Digital Converter for Electrochemical Impedance Spectroscopy Measurements," *IEEE Transactions on Biomedical Circuits and Systems*, vol. 11, no. 2. pp. 370–379, 2017.

[42]   C. Yang, S. R. Jadhav, R. M. Worden, and A. J. Mason, "Compact Low-Power Impedance-to-Digital Converter for Sensor Array Microsystems," *IEEE Journal of Solid-State Circuits*, vol. 44, no. 10. pp. 2844–2855, 2009.

[43]   W. Gao, S. Emaminejad, H. Y. Y. Nyein, S. Challa, K. Chen, A. Peck, H. M. Fahad, H. Ota, H. Shiraki, D. Kiriya, D.-H. Lien, G. A. Brooks, R. W. Davis, and A. Javey, "Fully integrated wearable sensor arrays for multiplexed in situ perspiration analysis," *Nature*, vol. 529, no. 7587, pp. 509–514, Jan. 2016.

[44]   D. Zhang, Y. Lu, Q. Zhang, L. Liu, S. Li, Y. Yao, J. Jiang, G. L. Liu, and Q. Liu, "Protein detecting with smartphone-controlled electrochemical impedance spectroscopy for point-of-care applications," *Sensors Actuators, B Chem.*, vol. 222, pp. 994–1002, 2016.

[45]   J. B. Pietzsch, L. A. Shluzas, M. E. Paté-Cornell, P. G. Yock, and J. H. Linehan, "Stage-Gate Process for the Development of Medical Devices," *J. Med. Device.*, vol. 3, no. 2, p. 21004, 2009.

[46]   A. Devices, "ADG608; ADG609; 3 V/5 V; 4-/8-Channel High Performance Analog Multiplexers; Data Sheet; Revision A," 1995.

[47]   "Texas Instruments, 'TLE206x, TLE206xA, TLE206xB, Excalibur JFET-Input High-Output-Drive uPower Operational Amplifiers, Datasheet,' Feb 1997-Revised May 2004."

[48]   T. Instruments and I. Sbos, "Precision , High-Speed Transimpedance Amplifier FEATURES EXCELLENT LONG-TERM V OS STABILITY," *Time*, no. September, 2007.

[49]   "Microchip Technology, 'Section 16. Analog to Digital Converter (ADC), Family Reference Manual, dsPIC33,' June 2012."

[50]   "Microchip technology, 'Section 22. Direct Memory Access (DMA), Family Reference Manual, dsPIC33F,' June 2011."

[51]   "Microchip Technology Inc, High-performance, 16-bit digital signal controller, dsPIC33FJXXXGPX06A/X08A/X10A datasheet," June 2006.," 2006.

[52]   Bluegiga, "Bluegiga BLE112 Datasheet," vol. 402, no. December, pp. 1–8, 1998.

[53]   "Gamry Instruments,Universal Dummy Cell 4, Operator's Manual." p. 5, 2016.

[54]   Gamry Instruments, "Potentiostat / Galvanostat / ZRA Operator 's Manual Reference 600," *ReVision*, 2005.

Appendix1: BLE Config

The BLE module was purchased from SiLabs and a development board was designed for testing out the features and data rate of the BLE module. The BLE chip requires its flash memory to be programmed with required hardware configurations and baud rate details. This was done using BGScript^{TM} available on SiLabs website. The following steps are to be followed when starting to program this Bluetooth Module.

1. Installing the tools: Download the latest install the Bluegiga Bluetooth Smart SDK from the Bluegiga web site.

2. Setting up the project: The project is started by creating a project file. The file is a simple XML formatted document and defines all the other files the included in the project.

3. Defining hardware configuration: The UART port configurations and baud rates are defined here.

4. Building a GATT based service database with profile toolkit: Every Bluetooth Smart device needs to implement a GAP service. The GAP service is very simple and consists of only two characteristics.

5. Writing a simple BGScript that defines the sensors functionality: The Cable Replacement Module available on the website is used here. BGScript uses an event-based programming approach. The script is executed when an event takes place, and the programmer may register listeners for various events

6. Compiling the GATT data base and BGScript into a binary firmware: When you want to test your project, you need to compile the hardware settings, the GATT data base and

BGScript code into a firmware binary file. The easiest way to do this is with the BLE Update tool that can be used to compile the project and install the firmware to a Bluetooth Smart Module using a CC debugger tools.

7. Installing the firmware into BLE112 or BLED112 hardware: Texas Instruments flash tool is used to install the firmware into the target device using the CC debugger

8. Testing it out

Appendix 2: UI Config

The first step is to configure the Bluetooth device to the computer to pair it. This is done by using a Python script that enables us to collect the data and save it in a text file. The Python script checks all serial ports for connectivity and connects a COM port for serial communication. This Python script is also integrated in the FlaskApp project and after the user interface is turned on, the pairing of BLE starts automatically. The following steps are taken to navigate and get started with the user interface.

1. The FlaskApp controller.py application is run. This displays a message in its output section "Running on http://127.0.0.1:5000/". This terminal also displays all requests and any error messages throughout the use of the program.

2. A web browser is opened and the address 127.0.0.1:5000 is entered. It displays the home page of the application.

3. This requires us to click to input parameters for the test.

4. Once the parameters are entered, they are passed into the BLE connectivity file, which starts pairing the device and once paired sends the input parameters to the microcontroller.

5. On the other side, the microcontroller is waiting for the input parameters and the start test command from the laptop. Once it receives this information in its receive buffer, it decodes the parameters and starts the test.

6. Data immediately transmits across the wireless medium and starts getting saved in the text file.

7. At the end of approximately 60 seconds, or the end of one test cycle, the test stops.

8. If the plot graphs button is pressed next, the FlaskApp next samples the data and displays the impedance magnitude and phase of the sensors in test.

Appendix 3: Parts, Services and Tools

For sourcing parts:

1. DigiKey was used to source majority of the components, both SMDs and through hole.

2. Mouser Electronics was used to source a few of the other components.

3. Amazon was used to source more readily available electronics like breadboards, wires etc.

Services:

1. OSH Park was used for all PCB manufacturing operations. All boards were two layered-boards.

2. Belittle Electronics was also considered for PCB manufacturing but not used.

Tools:

1. Eagle CAD was used for all schematic and board layout designs. A professional version of the software was purchased for this research purposes.

2. MPLABX IDE was used for programming Microchip's MCU, the dsPIC33F. An ICD3 debugger and programmer was used to physically connect to the computer running MPLABX for programming and verification.

3. FlaskApp was used for developing the entire user interface. This IDE was chosen because it developed both the front end and back end parts of the user interface making it easier to manage the project.

4. Python scripting language was used to program the entire user interface.

5. SmartSine was used to develop the sinusoidal waves tables for all the frequencies of the tests.